ELSEVIER

Tectonophysics 280 (1997) 267–293

TECTONOPHYSICS

Late Cretaceous, synorogenic, low-angle normal faulting along the Schlinig fault (Switzerland, Italy, Austria) and its significance for the tectonics of the Eastern Alps

N. Froitzheim *, P. Conti [1], M. van Daalen

Geologisch–Paläontologisches Institut, Universität Basel, Bernoullistr. 32, CH-4056 Basel, Switzerland

Received 9 July 1996; accepted 10 February 1997

Abstract

The Schlinig fault at the western border of the Ötztal nappe (Eastern Alps), previously interpreted as a west-directed thrust, actually represents a Late Cretaceous, top-SE to -ESE normal fault, as indicated by sense-of-shear criteria found within cataclasites and greenschist-facies mylonites. Normal faulting postdated and offset an earlier, Cretaceous-age, west-directed thrust at the base of the Ötztal nappe. Shape fabric and crystallographic preferred orientation in completely recrystallized quartz layers in a mylonite from the Schlinig fault record a combination of (1) top-east-southeast simple shear during Late Cretaceous normal faulting, and (2) later north-northeast-directed shortening during the Early Tertiary, also recorded by open folds on the outcrop and map scale. Offset of the basal thrust of the Ötztal nappe across the Schlinig fault indicates a normal displacement of 17 km. The fault was initiated with a dip angle of 10° to 15° (low-angle normal fault). Domino-style extension of the competent Late Triassic Hauptdolomit in the footwall was kinematically linked to normal faulting.

The Schlinig fault belongs to a system of east- to southeast-dipping normal faults which accommodated severe stretching of the Alpine orogen during the Late Cretaceous. The slip direction of extensional faults often parallels the direction of earlier thrusting (top-W to top-NW), only the slip sense is reversed and the normal faults are slightly steeper than the thrusts. In the western Austroalpine nappes, extension started at about 80 Ma and was coeval with subduction of Piemont–Ligurian oceanic lithosphere and continental fragments farther west. The extensional episode led to the formation of Austroalpine Gosau basins with fluviatile to deep-marine sediments. West-directed rollback of an east-dipping Piemont–Ligurian subduction zone is proposed to have caused this stretching in the upper plate.

Keywords: tectonics; synorogenic extension; low-angle normal fault; Alps; Austroalpine

1. Introduction

The Schlinig fault is the shallowly dipping contact between pre-Mesozoic basement of the Ötztal nappe above and Mesozoic sedimentary rocks of the Engadine dolomites (S-charl nappe) below (Fig. 1). It has gained some fame in the Alpine literature because it is spectacularly exposed, shows the superposition of basement on sedimentary rocks in a text-book manner, and has given rise to different interpretations and controversies among Alpine geologists. The kinematics and age of this fault are not only of local interest but greatly affect the tec-

* Corresponding author. Fax: +41 61 267-3613. E-mail: froitzheim@ubaclu.unibas.ch

[1] Present address: Direzione Rilevamento, Via Nuoro 3, 09046 San Vito (CA), Italy.

PII S0040-1951(97)00037-1

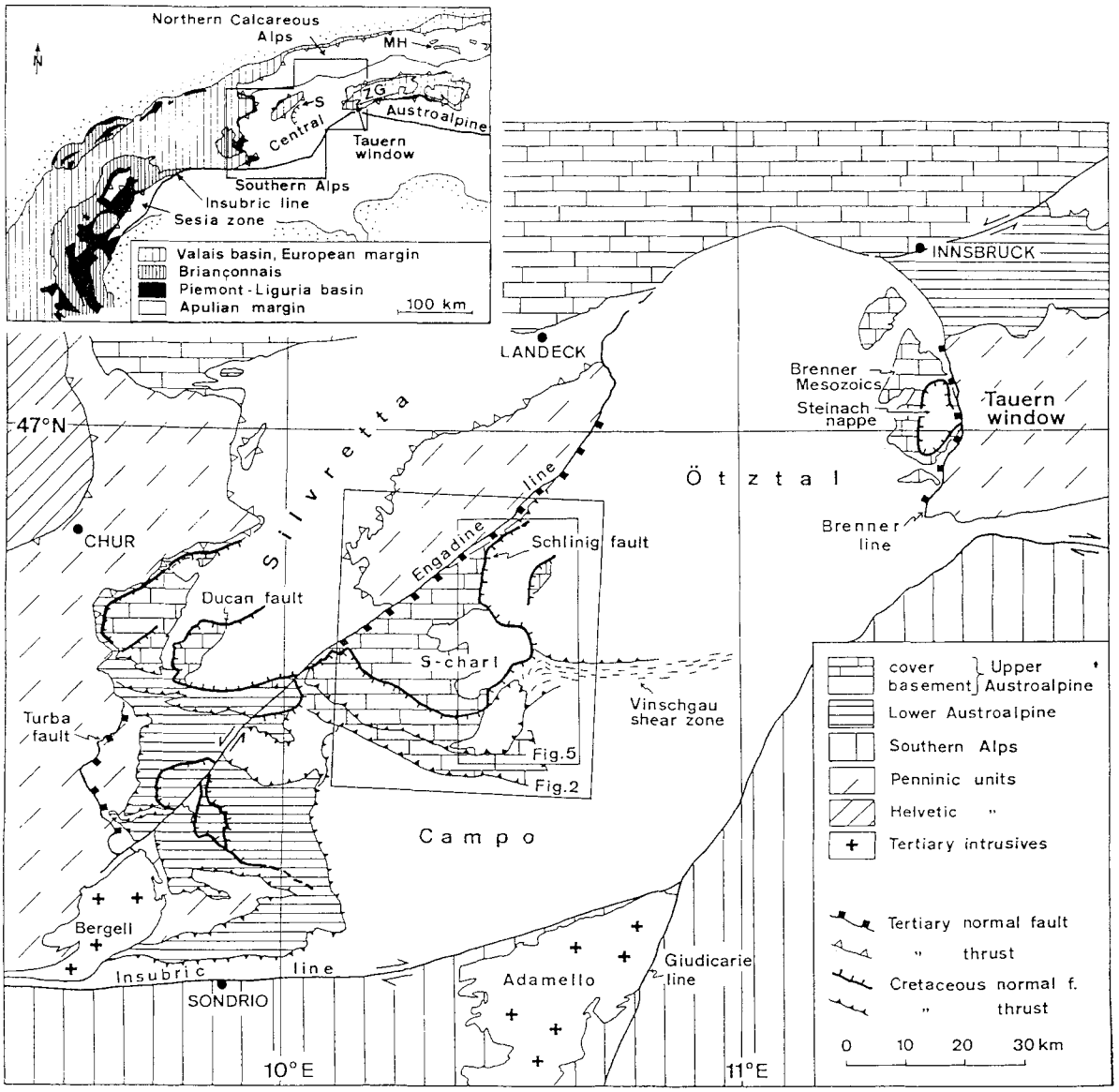

Fig. 1. Tectonic overview of the western part of the Eastern Alps. Inset: sketch map of the Alps showing palaeogeographic provenance of tectonic units. *MH* = Meliata–Hallstatt units; *S* = Schlinig fault; *ZG* = Zentralgneiss.

tonic interpretation of the western part of the Austroalpine nappe system. Hammer (1908) and Spitz and Dyhrenfurth (1914) interpreted the Schlinig fault as a W- to WNW-directed thrust of the Ötztal mass over the Engadine dolomites. They were criticized by Heim (1922) who postulated that the thrusting was directed northward. Trümpy (1980) and Thöni (1980a), among others, again inferred westward thrusting along the Schlinig fault. Both authors assumed that at least the late stages of thrusting occurred in the Tertiary period, postdating earlier, Late Cretaceous deformation and metamorphism, because the Schlinig fault truncated early folds of the Engadine dolomites and disturbed the zonation of Cretaceous-age metamorphism (Thöni, 1980a). Schmid and Haas (1989) studied an east–west-trending my-

lonite zone at the southern border of the Ötztal nappe in the Vinschgau valley, the Vinschgau shear zone (Fig. 1), and demonstrated that it accommodated a westward transport of the Ötztal nappe relative to the underlying Campo nappe, during the Cretaceous. They assumed that the Schlinig fault represented the continuation of the Vinschgau shear zone towards northwest into shallower levels of the crust. Consequently, they interpreted the Schlinig fault as a Cretaceous-age, top-west thrust.

In the following, we will present a kinematic study of the Schlinig fault between the Vinschgau valley to the south and the Reschen pass to the north, and of its southwestward prolongation, the Gallo fault (Fig. 2). The result of this study contradicts all of the above interpretations: the Schlinig fault is not a thrust, but a Late Cretaceous, top-southeast normal fault postdating earlier nappe imbrication. This has important implications for the tectonic history of the Austroalpine nappes.

2. Regional setting

The study area belongs to the western Austroalpine nappes. These originated from the southeastern margin of the Mesozoic Tethys ocean. They were stacked east-over-west in Late Cretaceous time and were later, during the Early Tertiary, thrust northward as one large thrust mass over the Penninic nappes. The latter are exposed in the Tauern and Engadine windows, framed by the overlying Austroalpine nappes. The sequence of deformation in the Austroalpine nappes of Graubünden was recently established as follows (Froitzheim et al., 1994; Fig. 3): Cretaceous deformation includes west- to northwest-directed nappe imbrication and associated folding (Trupchun phase, ca. 100–80 Ma), followed by ESE-directed asymmetric extension of the nappe stack (Ducan-Ela phase, ca. 80–67 Ma). Subsequently, in the Early Tertiary, the Austroalpine nappe stack was thrust northward over the Penninic nappes and folded around WNW–ESE axes (Blaisun phase, 50–35 Ma, possibly beginning earlier). This was followed by renewed E–W extension along the Turba mylonite zone located at the base of the Cretaceous nappe stack, contemporaneously with north–south shortening (Turba phase, ca. 35–30 Ma) (Dal Piaz et al., 1988). Finally, the nappe stack was mildly folded around SW–NE axes (Domleschg phase, ca. 30–25 Ma; von Blanckenburg, 1992), and dissected by the Engadine line, an oblique-slip fault which accommodated important block rotations (Figs. 1 and 2; Schmid and Froitzheim, 1993).

For this study, the following Austroalpine tectonic units are of interest (Figs. 1 and 2):

(1) The *Ötztal nappe* largely consists of Pre-Permian crystalline basement. Remnants of its Permo–Mesozoic cover are preserved near the eastern border of the nappe (Brenner Mesozoics). The Permo–Mesozoic rocks of Jaggl, often interpreted as a tectonic window through the Ötztal nappe (Hess, 1962; Stutz and Walter, 1983), represent, according to our results, another remnant of the sedimentary cover of the Ötztal nappe.

(2) The *S-charl nappe*, underlying the Ötztal nappe along the Schlinig fault, includes pre-Permian basement as well as Permian to Mesozoic cover rocks. The Permian to Middle Triassic part of the cover was folded and slightly imbricated together with the basement ('S-charl-Unterbau'; Spitz and Dyhrenfurth, 1914), whereas the Upper Triassic Hauptdolomit was detached from the underlying rocks along the evaporite-bearing Raibl Formation, and deformed independently ('S-charl-Oberbau').

(3) The *Umbrail–Chavalatsch Schuppenzone* (UCS) represents an imbricated stack of crystalline basement and Mesozoic, mostly Upper Triassic, sedimentary rocks (Schmid, 1973). The basement rocks are lithologically identical to certain rock types of the Ötztal nappe. Within the UCS, the basement/sediment ratio decreases westward. Hence, the whole UCS appears as a zone of tectonic interfingering of the Ötztal basement, dominating to the east, with a stack of sediment thrust sheets to the west. The largest of these thrust sheets is the *Quattervals nappe*, consisting almost exclusively of Upper Triassic carbonates. To the north, the Quattervals nappe and the UCS overlie the S-charl nappe along the southwest- to southeast-dipping Gallo line. In the northern part of the study area, the Triassic rocks of *Piz Lad* near Nauders occupy a similar position as the sedimentary constituents of the Umbrail–Chavalatsch Schuppenzone (Fig. 2). To the northeast, the Piz Lad sediments rest along a tectonic contact on Ötztal basement rocks. To the south, the sediments are overlain by the main mass of Ötztal

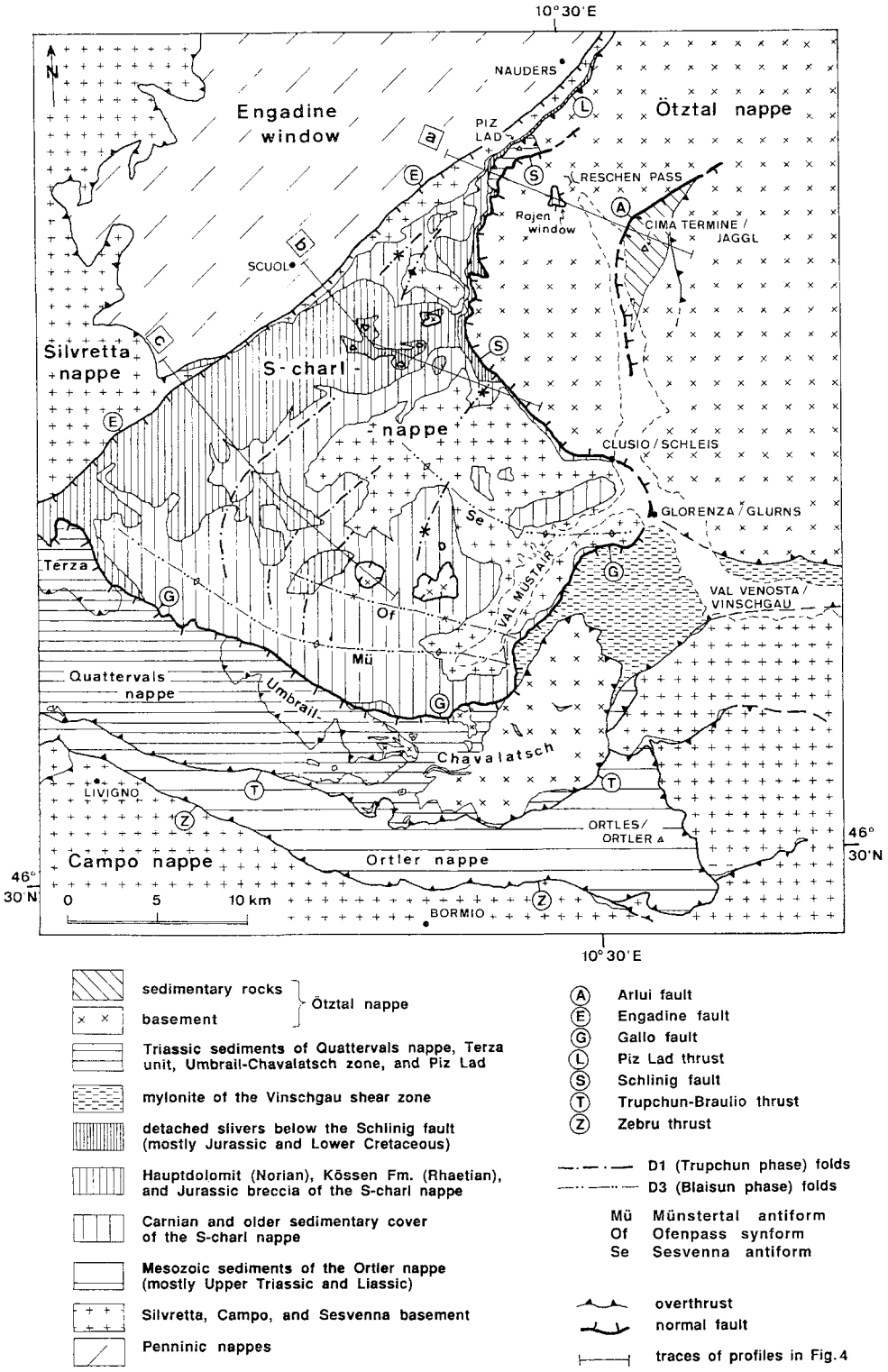

Fig. 2. Tectonic map of the study area.

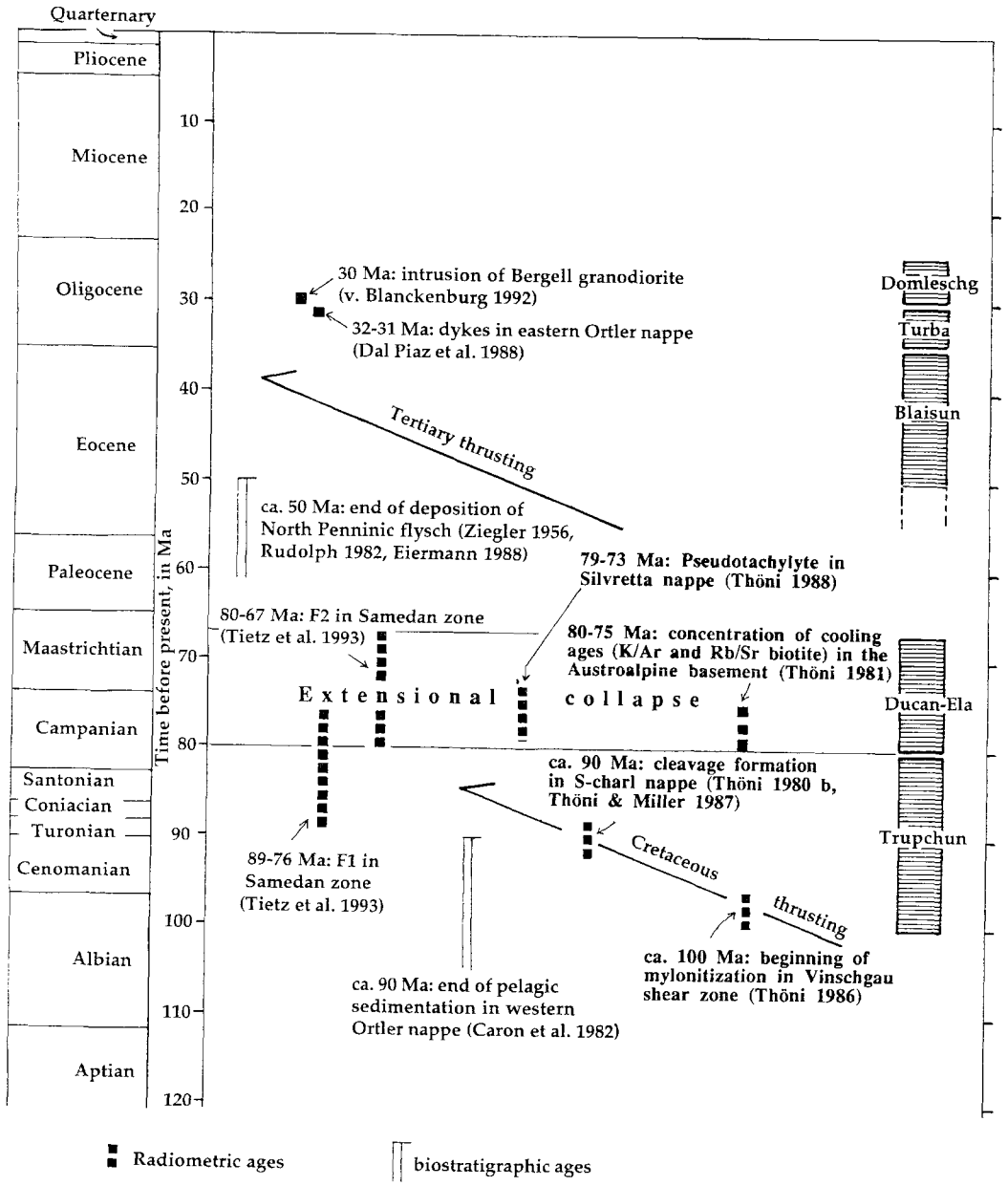

Fig. 3. Time table for Cretaceous and Tertiary deformation of the western Austroalpine nappes. After Froitzheim et al. (1994), slightly modified and complemented.

basement, along the Schlinig fault. Thus, Piz Lad appears as a wedge of Triassic sediments intercalated between Ötztal basement rocks above and below. To the northwest, the Piz Lad sediments directly overlie cover rocks of the S-charl nappe along a thrust ornamented by slivers of basement (Torricelli, 1956).

(4) The *Ortler nappe* consists of Permo–Triassic to Cretaceous sedimentary rocks and underlies the Quattervals nappe and the UCS along the Trupchun–Braulio thrust (Schmid, 1973; Conti et al., 1994).

(5) The *Campo nappe* consists of Pre-Mesozoic basement and is divided from the overlying Ortler

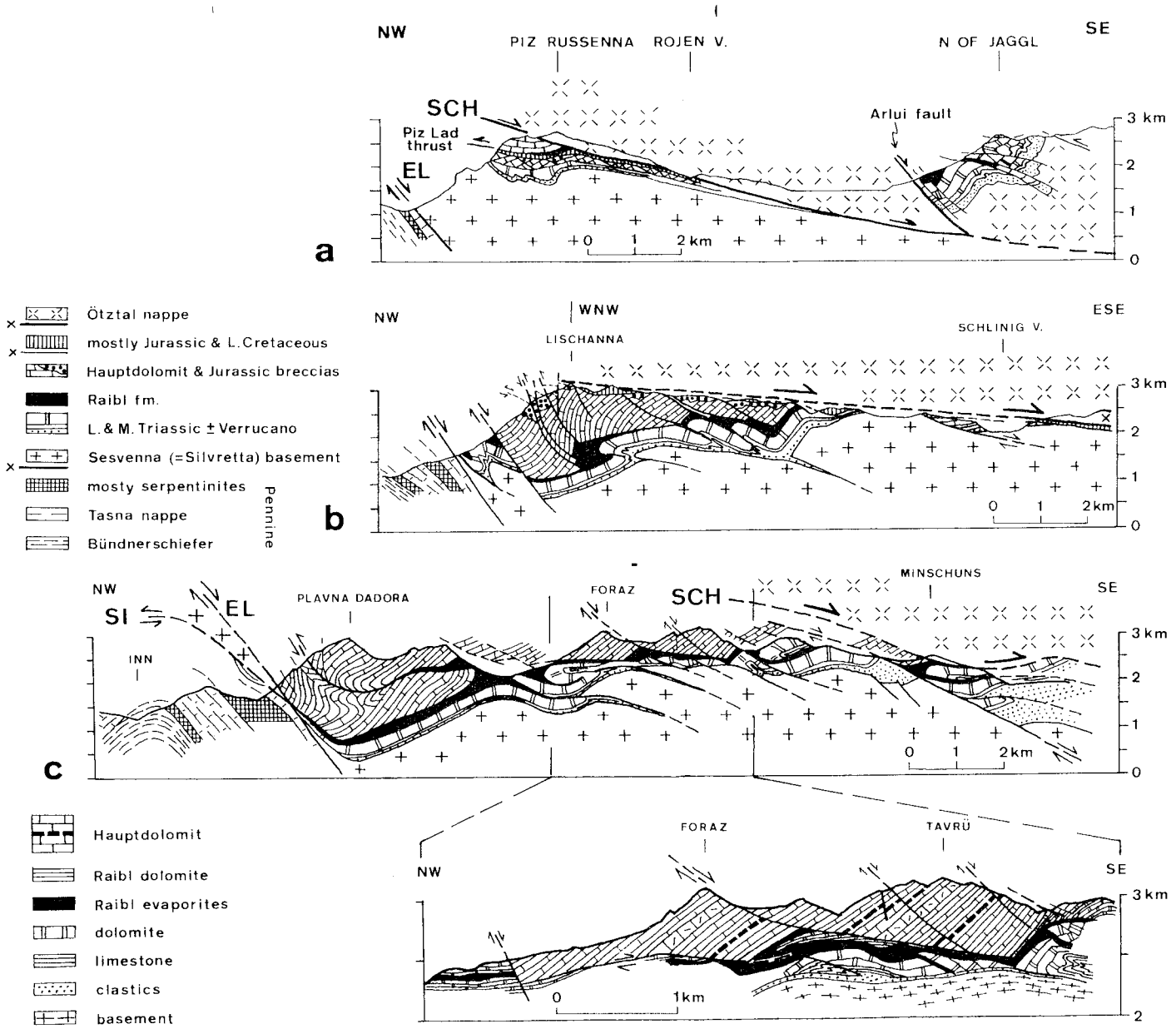
a
NW
SE
PIZ RUSSENNA
ROJEN V.
N OF JAGGL
SCH
Piz Lad thrust
EL
Arlui fault
3 km
2
1
0
0 1 2km
b
NW
WNW
ESE
LISCHANNA
SCHLINIG V.
3 km
2
1
0
0 1 2km
c
NW
SI
EL
PLAVNA DADORA
FORAZ
SCH
MINSCHUNS
SE
INN
3 km
2
1
0
0 1 2km
FORAZ
TAVRÜ
NW
SE
3 km
2
0 1km
Ötztal nappe
mostly Jurassic & L.Cretaceous
Hauptdolomit & Jurassic breccias
Raibl fm.
L.& M.Triassic ± Verrucano
Sesvenna (=Silvretta) basement
mosty serpentinites
Tasna nappe
Bündnerschiefer
Pennine
Hauptdolomit
Raibl dolomite
Raibl evaporites
dolomite
limestone
clastics
basement

nappe by an Alpine thrust (Zebrù thrust; Conti, 1992, 1994).

(6) The *mylonite of the Vinschgau shear zone* is partly derived from pre-Permian basement, partly from Permo–Triassic sedimentary rocks (Schmid and Haas, 1989). This thick layer of mylonite is found between the Ötztal nappe and the UCS above, and the S-charl nappe, Ortler nappe, and Campo nappe below.

The term 'Engadine dolomites' summarizes the sedimentary portions of the S-charl, UCS, Quattervals and Ortler nappes, cropping out in the form of a triangle between the Engadine line, the Ötztal, and the Campo nappe (Fig. 2).

3. Results

3.1. Fault geometry

The Schlinig fault is exposed over a N–S distance of 20 km between the Reschen pass in the north and Clusio/Schleis in the Vinschgau valley, in the south (Figs. 2 and 4). Near Clusio, the fault disappears under the Quaternary fill of the Vinschgau valley. In the North, the fault leaves the sediment–basement contact and becomes an intra-basement fault in the Ötztal nappe. The eastward extension of this fault within the Ötztal nappe has not yet been mapped. Between the Reschen pass and Clusio/Schleis, the Schlinig fault describes a westward convex arc. This is due to a listric shape of the fault which dips 16° northeast in the south, 8° to 9° east in the middle part, and 17° southeast in the north (see contour map in Stutz and Walter, 1983, from which also the dip angles were taken). Measured parallel to the movement direction (see below) between Piz Rims and Clusio/Schleis (Figs. 5 and 6), the dip angle is 7.5°. Erosion through the Schlinig fault has created a tectonic window of S-charl-nappe sediments surrounded by Ötztal basement rocks in the Rojen valley (Rojen window, Fig. 2), and several isolated klippen of Ötztal rocks on top of S-charl-nappe sediments farther west.

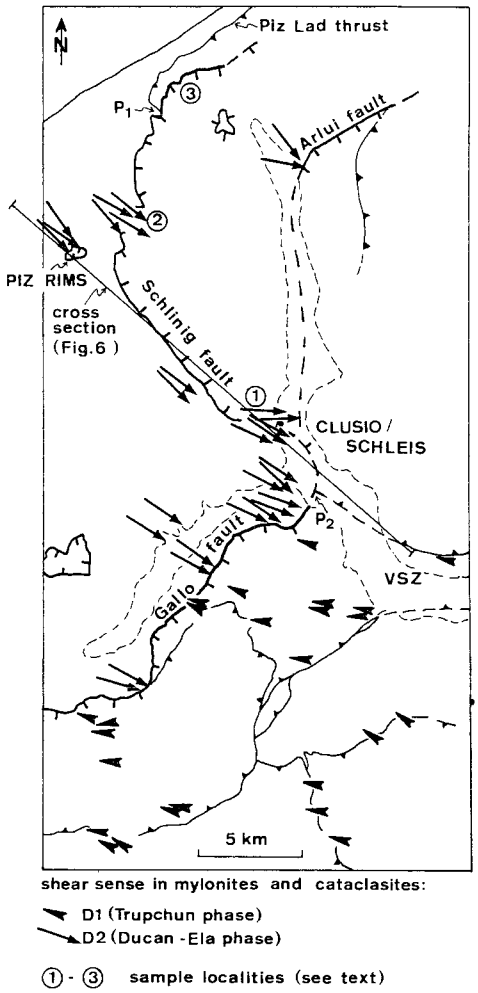

Fig. 5. Map showing shear direction and shear sense in mylonites and cataclasites from the Schlinig–Gallo fault system and surrounding area. Earlier, Trupchun-phase mylonites are abundant in the hanging wall of the normal fault system, whereas in the footwall, they were largely overprinted by top-SE shear. P_1 and P_2 are intersection points of the Schlinig fault with the basal thrust of the Ötztal nappe in the footwall and in the hanging wall, respectively. *VCS* = Vinschgau shear zone.

The Ötztal nappe in the hanging wall consists of gneiss and mica schist with amphibolite layers, discordantly cut by the Schlinig fault (see Fig. 1

Fig. 4. Cross-sections through the Engadine dolomites and the overlying Ötztal nappe. Traces of cross sections: see Fig. 2. Cross-sections (b) and (c) are from Schmid and Haas (1989), with the only modification of the slip sense along the Schlinig fault, which is top-SE according to this study. *SCH* = Schlinig fault, *EL* = Engadine line, *SI* = basal thrust of the Silvretta nappe.

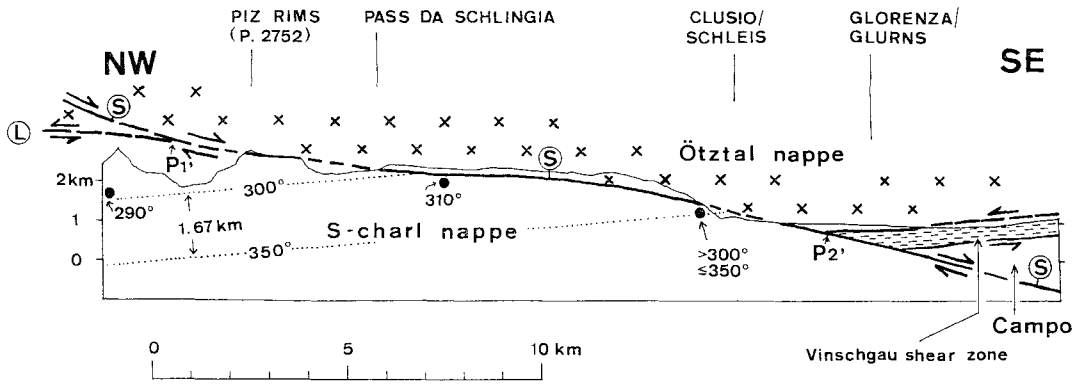

Fig. 6. Cross-section parallel to the slip direction of the Schlinig fault. Trace of section in Fig. 5. $P_{1'}$ and $P_{2'}$ are intersection points of the Schlinig fault with the basal thrust of the Ötztal nappe, projected into the section. Temperature estimates for the footwall are from a combined illite crystallinity/vitrinite reflectance study of Kürmann (1993). 300°C and 350°C isograds were drawn under the assumption of a 30°C/km geotherm. S = Schlinig fault. For further explanation see text.

in Hammer, 1908). The regional amphibolite-grade metamorphism of these rocks is Hercynian in age (Thöni, 1980b). The Alpine deformation of the Ötztal rocks is restricted to the lowermost few metres where a cataclastic or, in the southernmost exposed part of the Schlinig fault, mylonitic overprint of the Hercynian structures is observed. The footwall of the Schlinig fault mainly consists of Mesozoic sediments of the S-charl nappe or, in the northernmost part, the Piz Lad unit. An older, pre-Schlinig-fault deformation of the S-charl nappe is represented by SW–NE-striking, northwest-facing folds of the Trupchun phase which deform the sediments and the basement–sediment contact in the footwall but are truncated by the Schlinig fault (Stutz and Walter, 1983; Fig. 2). In the area northwest of Clusio/Schleis (Figs. 2 and 4b), the thickness of the sediments decreases towards the southeast so that the Ötztal nappe almost directly rests on the basement of the S-charl nappe. In this area, a mylonitic, Schlinig-fault-related overprint of the footwall basement rocks is not restricted to the vicinity of the fault itself but is observed over a structural thickness of several hundred metres into the footwall. Kinematic analysis of fault rocks (see below) revealed that the Gallo fault (Böse, 1896; Hess, 1953; Schmid, 1973; Conti, 1994; Fig. 2) represents the southwestward prolongation of the Schlinig fault. The Gallo fault separates the S-charl nappe to the north from the overlying Umbrail–Chavalatsch-Schuppenzone and Quattervals nappe, to the south. It generally dips south (SW in the western part and SE in the eastern part). It truncates earlier thrust faults and recumbent folds of the Trupchun phase (see figs. 15 and 16 of Schmid, 1973) and is itself, in its eastern part, gently folded around later, open, WNW–ESE-striking anti- and synforms which are ascribed to the Blaisun phase (Fig. 2: Münstertal antiform, Ofenpass synform; Schmid, 1973; Conti, 1994). We assume that the Gallo and Schlinig faults are connected around the hinge of the east-dipping Sesvenna antiform, also formed during the Blaisun phase (Fig. 2). The connection is buried under the Vinschgau valley fill.

In addition to the Schlinig and Gallo faults, fault rocks were also sampled along the Arlui fault (Figs. 2 and 4a). This is the moderately to steeply southeast-dipping contact between Permo–Mesozoic rocks of Jaggl, to the southeast and above the fault, and Ötztal basement, to the northwest and below.

3.2. Kinematic analysis of mylonites and cataclasites

Although the Schlinig fault is well visible from a distance through the contrast between gneiss in the hanging wall and sedimentary rocks in the footwall, good outcrops of the fault contact itself are rare. The best outcrops along the fault are locations 1 to 3 (see Fig. 5) described below.

Location 1 is an approximately 100 m thick section of mylonites exposed on the northern side of the stream west of Clusio/Schleis (Swiss coordi-

nates 835.200/176.150). These mylonites are derived from basement gneisses of the S-charl nappe, sericite phyllite (representing Permian volcaniclastic rocks), Lower Triassic sandstone, and Middle Triassic carbonate rocks. Mylonitized Ötztal gneiss occurs in the uppermost part of the section. Triassic sediments and older rocks are imbricated, producing stratigraphic repetitions. The mylonites exhibit a well developed foliation dipping shallowly north to east, and a stretching lineation in quartz-rich layers which is oriented SE to ESE. Additionally, a weak post-mylonitic crenulation, subparallel to slightly oblique with respect to the stretching lineation, is observed in mica-rich layers. In the field, the shear sense of the mylonites is difficult to assess; only indistinct shear band/foliation relationships and occasional porphyroclast systems reveal a top-to-the-SE shear sense (Fig. 7a).

Thin sections perpendicular to the foliation and parallel to the lineation show abundant shear sense criteria (Fig. 7b–e), including shear band/foliation relationships (Fig. 7b), S–C fabrics (Fig. 7c), asymmetric porphyroclast systems (Fig. 7d), asymmetric mica fish (Lister and Snoke, 1984), and grain-shape preferred orientations in thin quartz layers (Fig. 7e). The porphyroclasts are feldspar-, quartz-, and tourmaline-grains. Generally the observed porphyroclast systems are of the σ-type (Passchier and Simpson, 1986). The shear sense indicated by the criteria listed above is consistently top-to-the-southeast (Fig. 5).

Quartz is observed in thin layers between mica-rich layers and as former porphyroclasts in a sericite–feldspar–quartz-rich matrix. Quartz is completely dynamically recrystallized. The grain size in the recrystallized layers is approximately 100 μm. The shape of the former porphyroclasts can still be discerned, but they now consist entirely of recrystallized grains. The shape fabric of the recrystallized grains in the thin quartz layers indicates top-SE shear sense (Fig. 7e).

Location 2 is about 10 km farther to the northwest (Swiss coordinates 828.125/186.00). The footwall in this area consists of mylonitized, Middle Triassic limestone with an E- to SE-dipping foliation and a pronounced ESE- to SE-striking stretching lineation. Foliated, basement-derived cataclasite occurs in a 10 to 20 m thick layer at the base of the overlying Ötztal gneiss. Typically, these cataclasites have a main foliation dipping shallowly SE and abundant shear bands, also dipping SE but at a higher angle. A slickenside lineation is formed on the foliation and on the shear bands. This lineation is oriented SE–NW, perpendicular to the intersection of foliation and shear bands. Hence, the lineation, foliation, and shear bands are interpreted to be all related to the same deformation process that formed the cataclasites. From the asymmetry of the shear band-foliation relationship, a top-to-the-SE sense of shear is clearly recognized in the field.

In thin section, three types of planar elements are observed: (1) a foliation ('s' in Fig. 7f) defined by mica grains, elongated fragments of chloritized and sericitized gneiss protolith, and thin layers of ultracataclastic, very fine-grained material; (2) shear surfaces with ultracataclastic material, oriented parallel to the Schlinig fault ('c' in Fig. 7f); (3) shear bands, inclined with respect to the Schlinig fault. A slightly sheared and recrystallized pseudotachylyte vein was observed in one sample. Criteria on the microscopic scale (S–C structure, foliation/shear band relations, asymmetric clasts) clearly confirm the top-SE shear sense.

Quartz is mainly observed as porphyroclasts embedded in a fine-grained foliated matrix of feldspar, white mica, and quartz. The quartz porphyroclasts exhibit older (pre-Alpine) microstructures formed by grain boundary migration recrystallization, a mechanism which is active at elevated temperatures (Guillopé and Poirier, 1979; Drury and Urai, 1990), higher than the temperatures reached during the Alpine orogeny in this area. This former, higher-temperature deformation phase is responsible for the large bulges and serrated grain boundaries observed inside the porphyroclasts. These older microstructures are overprinted by the colder deformation during movement along the Schlinig fault. Quartz porphyroclasts and layers show strong undulatory to patchy extinction, deformation bands, and subbasal deformation lamellae. The latter usually indicate high flow stresses (Avé Lallemant and Carter, 1971; Drury, 1993). The initiation of dynamic recrystallization is observed along narrow bands with newly recrystallized grains (size 20 μm, see Fig. 7g), but completely recrystallized quartz layers as observed at location 1 are not present. This indicates lower temperature during deformation at location 2 as compared to location 1.

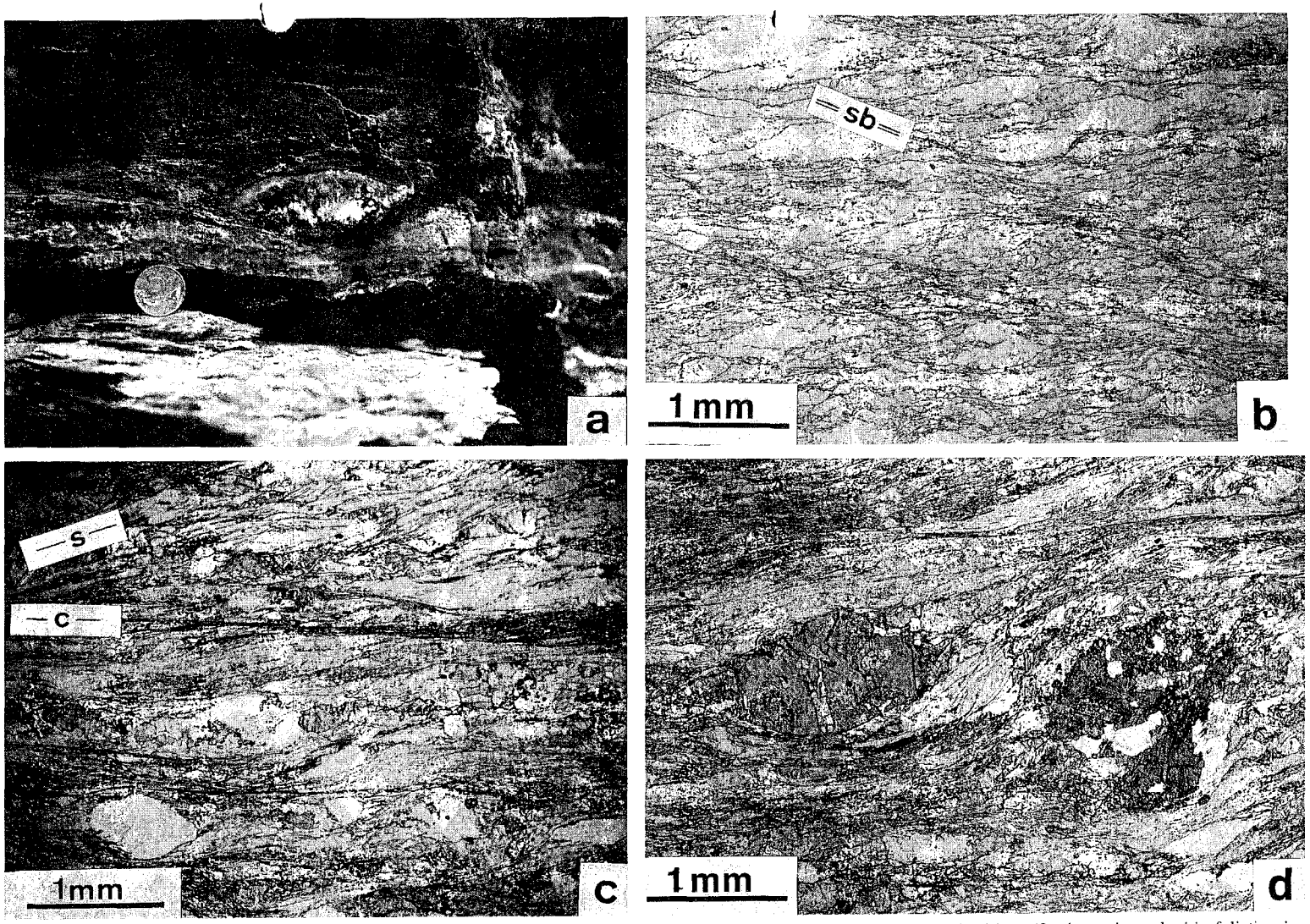

Fig. 7. Shear-sense indicators and quartz microstructures in mylonites and cataclasites from the Schlinig fault. In photographs (a) to (f), the main mylonitic foliation is horizontal and NW is to the left. (a) Quartz nodule forming a σ-type porphyroclast system in mylonite derived from Triassic carbonatic sandstone (Fuorn Formation). Asymmetry indicates dextral (top-SE) shear sense. Diameter of coin is 2 cm. Loc. 1 near Clusio/Schleis. (b) Mylonite derived from Ötztal basement rock. Shear bands (*sb*) indicate dextral (top-SE) shear sense. Plane-polarized light. Loc. 1 near Clusio/Schleis. (c) Mylonite derived from Triassic carbonatic sandstone (Fuorn Formation). S–C structure indicates dextral (top-SE) shear sense. Plane-polarized light. Loc. 1 near Clusio/Schleis. (d) Mylonite derived from Triassic carbonatic sandstone (Fuorn Formation). Asymmetric pressure shadows around two porphyroclasts of detrital tourmaline indicate dextral (top-SE) shear sense. Plane-polarized light. Loc. 1 near Clusio/Schleis.

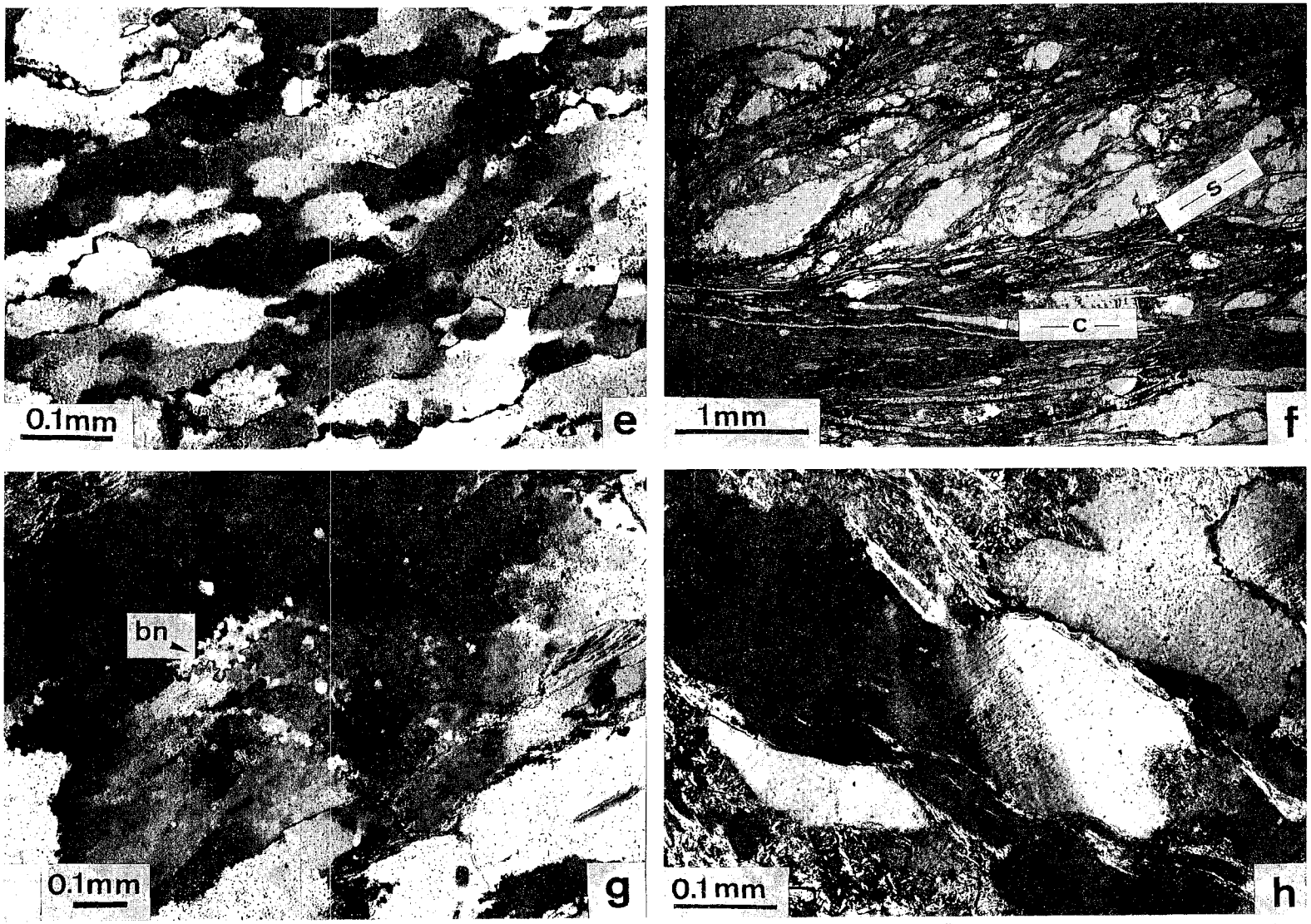

Fig. 7 (continued). (e) Dynamically recrystallized quartz from a foliation-parallel quartz layer in a mylonite derived from Ötztal basement rock. Note obliquity of grain shape with respect to the mylonite foliation (horizontal), indicating dextral (top-SE) shear. Occurrence of subgrains within larger recrystallized grains indicates subgrain rotation to be the dominant recrystallization mechanism. Crossed polars. Loc. 1 near Clusio/Schleis. (f) Foliated cataclasite derived from Ötztal gneiss. S–C structure indicates dextral (top-SE) shear sense. Plane-polarized light. Locality 2. (g) Incipient recrystallization of quartz in cataclasite derived from Ötztal gneiss. Large old quartz grains show patchy extinction and bands of small new grains; *bn* = bulge nucleation along an old grain boundary. Crossed polars. Locality 2. (h) Old quartz grains in

Location 3 is still farther north, southwest of Piz Lad (Swiss coordinates 830.388/191.787). Here, the footwall is formed by Upper Triassic Hauptdolomit of the Piz Lad unit. Cataclastic deformation of Ötztal basement rocks is restricted to a thin zone of 2 to 3 m (Schmid and Haas, 1989). Differently from location 2, foliation, lineation, and shear bands are not well developed and do not yield a consistent shear sense. Again the pre-Alpine deformation microstructures are observed in the quartz porphyroclasts and are clearly overprinted by the later colder deformation phase. This is indicated by incipient bulge nucleation observed on the old, large bulges. Furthermore, the quartz grains have subbasal deformation lamellae, some Böhm lamellae, and subgrain boundaries parallel to the prism planes, corresponding to the deformation bands described by Carter et al. (1964) (Fig. 7h). There is no evidence for recrystallization of quartz, which indicates still lower temperatures as compared to location 2.

3.2.1. Gallo line

Along the eastern portion of the Gallo line, a layer of mylonite is found in the uppermost part of the footwall. The protoliths are basement gneiss and Permo–Triassic volcaniclastic rocks. The foliation of the mylonites dips shallowly southeast, and the stretching lineation is oriented parallel to the dip direction, SE to ESE (Fig. 5). Quartz microstructures are very similar to those from the southern part of the Schlinig fault (loc. 1), indicative of lower-greenschist-facies conditions during deformation. The shear sense in the mylonites is consistently top-southeast. Along the western, NW–SE-striking portion of the Gallo line (outside the area of Fig. 5), both sides of the fault are formed by Triassic sediments, mainly dolomite. The deformation of the wall rocks is cataclastic in this area. Slickenside lineations along the fault are generally horizontal and NW–SE oriented, but indications of the slip sense could not be found.

3.2.2. Arlui fault

Foliated cataclasites and lower-greenschist-facies mylonites derived from Ötztal basement rocks were also found along the Arlui fault (Figs. 2 and 4a, and Fig. 5). Foliation/shear band relations, S–C structures, asymmetric porphyroclast systems, and mica fish in these fault rocks consistently yield a southeast-side-down sense of displacement. Triassic dolomite belonging to the Permo–Mesozoic successions of Jaggl, directly overlying these footwall-derived fault rocks, is cut by numerous top-east normal faults, also indicating normal displacement along the Arlui fault.

The study of the fault rocks yielded the following main results: (1) the shear sense along the Schlinig fault and the eastern part of the Gallo fault is consistently top-SE to top-ESE, with the exception of the northernmost locality 3 along the Schlinig fault where shear sense could not be determined; and (2) the microstructures of quartz in the fault rocks indicate a systematic northwestward decrease of the maximum deformation temperature. Taken together, the top-southeast shear sense, the overall eastward dip of the fault, and the increase of syn-deformation temperature in the transport direction clearly document the normal fault character of the Schlinig fault. Obviously, this normal fault movement must have postdated nappe imbrication, because basement rocks overlie Mesozoic sediments along the fault. The Gallo fault prolongates the Schlinig fault to the southwest. The top-southeast shear sense of the Schlinig fault is incompatible with the consistent top-west shear sense documented for the Vinschgau shear zone by Schmid and Haas (1989). Therefore, the latter cannot represent the prolongation of the Schlinig fault towards deeper crustal levels but represents an older Alpine shear zone, truncated by the Schlinig fault (see Fig. 6).

The Arlui fault is also a top-southeast normal fault and is interpreted as a hangingwall splay of the Schlinig fault (Fig. 4a). Consequently, the Jaggl Permo–Mesozoic rocks do not, according to our results, represent a window of the S-charl-nappe cover underlying the Ötztal nappe, as was often assumed (Hess, 1962; Thöni, 1973, 1980a; Stutz and Walter, 1983; Schmid and Haas, 1989), but a piece of Ötztal-nappe cover (Staub, 1937) thrown down towards the southeast along the Arlui normal fault.

3.3. Shape fabric and crystallographic preferred orientation of quartz

Shape fabric and crystallographic preferred orientation were analyzed quantitatively in a sample from

location 1 along the Schlinig fault (E409). Both the shape fabric and the crystallographic texture turned out to be strongly influenced by later, post-mylonitic, NNE–SSW-directed shortening (Blaisun phase), not visible on the hand specimen. In thin sections perpendicular to foliation and stretching lineation, however, mica-rich layers exhibit a crenulation resulting from this shortening (see Fig. 8a).

3.3.1. Shape preferred orientation (SPO)

The SPO was analyzed in three sections (Fig. 8): (1) parallel to lineation and normal to foliation (X–Z section), (2) normal to lineation and foliation (Y–Z section), and (3) parallel to lineation and foliation (X–Y section). In the geographic reference frame, the foliation dips 12° ESE (107°), and the stretching lineation (X direction) plunges ESE (103°) at an angle of 12°. SURFOR and PAROR methods of shape analysis (Panozzo, 1983, 1984) were applied. The three-dimensional shape fabric is unusual for a mylonite and can be explained by two successive deformation events.

The axial ratio of the elongated grains in the X–Z section (E409A) is 1.95 calculated by PAROR. In this section the grain long axes distribution (PAROR) has its maximum oriented oblique with respect to the foliation plane by 20° (Fig. 8c). The maximum of the grain boundary distribution (SURFOR) is inclined 25° with respect to the foliation plane (Fig. 8c). The obliquity of the maxima with respect to the foliation is consistent with top-ESE shear.

The axial ratio of the quartz grains in the Y–Z section (E409D) is 1.57. The SPO suggests flattening parallel to the Y axis and extension parallel to the Z axis. The maximum of the long axes of the grains is inclined 80° to the foliation. The maximum of the preferred orientation of the grain boundaries is inclined 90° to the foliation. This cannot be explained by the mylonitic shearing because from this we would expect the grains to be elongated parallel to the foliation. Instead, these microstructures are consistent with the later compressional event (Blaisun phase).

Section E409F, the X–Y section parallel to the foliation, has an axial ratio of 1.76. The maxima of the preferred orientations of the grain long axes and of the grain boundaries are subparallel to the macroscopically visible stretching lineation, with a slight deviation which is anticlockwise for the grain long axes and clockwise for the grain boundaries.

As argued above, the non-coaxial, top-ESE mylonitic shearing (Ducan-Ela phase) is likely to be responsible for the oblique orientation of the grain long axes with respect to the foliation in section E409A. During the following coaxial, N–S-directed shortening (Blaisun phase), a microscopic crenulation developed with axes subparallel to the stretching lineation produced by the Ducan-Ela phase. It is suggested that this shortening event accounts for the microstructure in section E409D but did not obliterate the obliquity of the grains with respect to the foliation in section E409A.

3.3.2. Crystallographic preferred orientation (CPO)

Quartz CPO was measured in section E409A (X–Z section) with the X-ray texture goniometer and the U-stage. With respect to the foliation and macroscopically visible stretching lineation, the measurements yielded an unusual type of texture. From the field observations, the shear sense criteria in the X–Z plane, and the measured SPO, this section was supposed to contain the principal kinematic direction. The a-axis maxima, however, are perpendicular to the stretching lineation (Fig. 9a). By rotating the pole figure 90° around an axis normal to the foliation, it becomes clear that section E409D (perpendicular to lineation) contains the kinematic reference frame for that part of the deformation which led to the present quartz CPO. Fig. 9b shows the rotated pole figures. The c-axis pole figure is almost symmetric and resembles a type II cross-girdle (Lister, 1977; Schmid and Casey, 1986) or two-girdle pattern (Sander, 1970). We assume that this texture was formed by coaxial NNE–SSW shortening in the Blaisun phase. The deviation from a normal type II cross-girdle (compare Schmid and Casey, 1986) may be explained by a preexisting texture that formed during the top-ESE shearing and was not completely obliterated during the N–S shortening. The above suggests that the quartz CPO reflects two successive deformation phases, which is quite unusual. According to Lister and Williams (1979), the skeletal outline of a pattern of preferred orientation will only remember the last strain increment. In our case, the incomplete obliteration of the older texture is understandable because the overprinting deformation was rather weak.

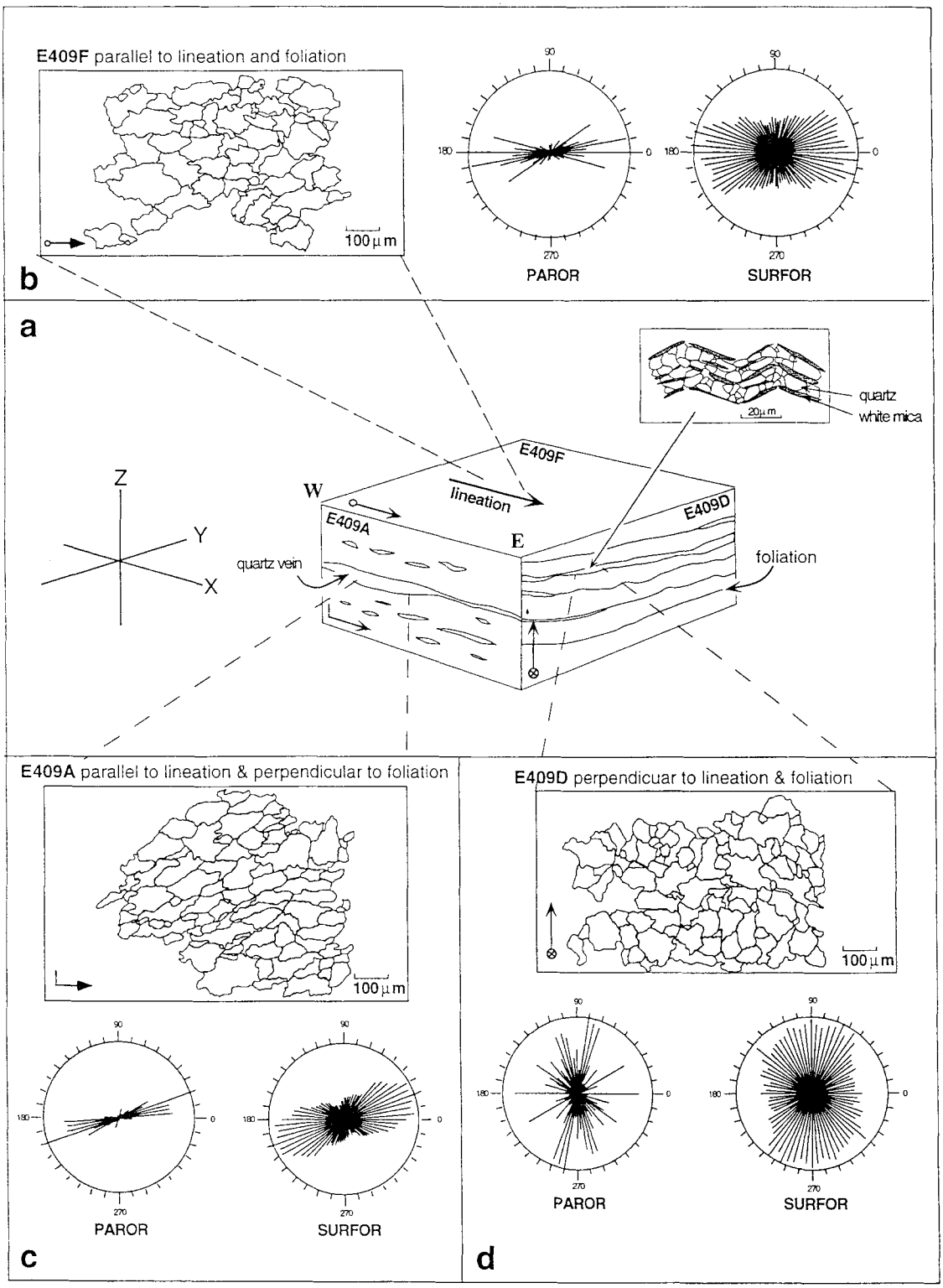
E409F parallel to lineation and foliation
100 µm
90
180
0
270
PAROR
SURFOR
b
a
quartz
white mica
20µm
E409F
lineation
W
E
E409A
E409D
quartz vein
foliation
Z
Y
X
E409A parallel to lineation & perpendicular to foliation
100 µm
PAROR
SURFOR
c
E409D perpendicuar to lineation & foliation
100 µm
PAROR
SURFOR
d

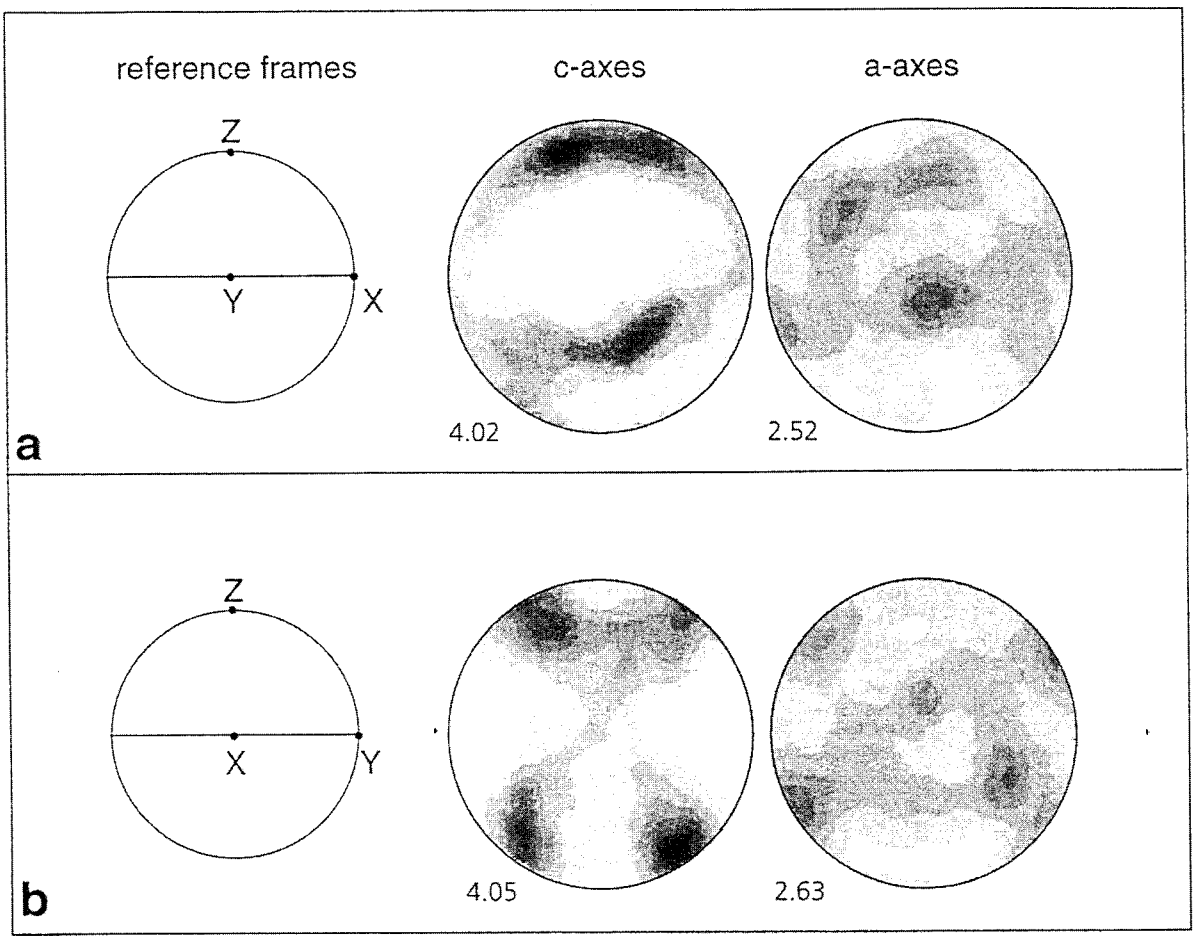

Fig. 9. (a) Quartz *c*-axis and *a*-axis pole figures as measured in section E409A, the *X–Z* section of the mylonitic deformation. W is to the left. The *c*-axis girdle does not pass through the center of the stereonet, and the *a*-axis maxima are at high angles to this section. (b) Pole figures after a 90° rotation around *Z*, that is, viewed in the *Y–Z* section. N is now to the left. *a*-axis maxima are at the periphery now, and *c*-axes show a type-II cross girdle, interpreted as indicating post-mylonitic coaxial shortening in the *Y* direction, that is, perpendicular to the mylonitic shear direction (*X*). Numbers below the pole figures give the intensity of the maxima (e.g. 4.05 times uniform).

From the analysis of the SPO and the CPO and the comparison of the two, the following conclusions can be drawn. (1) Both SPO and CPO can best be explained by two successive deformation events, the first of which was noncoaxial, top-ESE shearing (Schlinig normal fault, Ducan-Ela phase), and the second was coaxial, NNE–SSW shortening (Blaisun phase). (2) Although the N–S shortening is macroscopically invisible in this particular sample, it significantly modified the SPO and CPO.

Fig. 8. Shape fabrics in a dynamically recrystallized quartz vein from a Schlinig-fault mylonite. (a) Sketch of the sample, illustrating the relationship between the macroscopic stretching lineation developed during Schlinig fault movement and microscopic crenulation developed during later N–S shortening. (b) Quartz grain boundaries in the *X–Y* section (E409F) and resulting PAROR and SURFOR diagrams. (c) Shape fabric in *X–Z* section (E409A). (d) Shape fabric in *Y–Z* section (E409D). Foliation is always E–W in the rose diagrams. PAROR rose diagrams represent the orientation distribution of the long axes of the grains, SURFOR diagrams represent the grain boundary orientation distribution.

3.4. Amount of displacement across the Schlinig fault

Since extension along the Schlinig fault postdates nappe imbrication, the offset of thrust faults by the normal fault may be used for determining the amount of displacement. The basal thrust of the Ötztal nappe is exposed in the hanging wall and in the footwall of the Schlinig fault. In the hanging wall it is represented by the Vinschgau shear zone, along the northern side of the Vinschgau valley. The top of this north-dipping shear zone is truncated by the Schlinig fault in the vicinity of Glorenza/Glurns, under the Quaternary valley fill (P_2 in Fig. 5). In the footwall, the thrust at the base of the Piz Lad unit (Piz Lad thrust, Fig. 2) is interpreted to represent the basal thrust of the Ötztal nappe. West of Piz Lad, this thrust places Triassic rocks of the Piz Lad unit on Jurassic rocks of the S-charl nappe (Fig. 4a). Slivers of basement rocks occur along the thrust. Farther northeast, the thrust is between Ötztal basement rocks above and S-charl basement below, with a thin layer of mylonitized Mesozoic sediments in between. This Piz Lad thrust is truncated by the Schlinig fault at P_1 (Fig. 5). Fig. 6 is a cross-section parallel to the movement direction of the Schlinig normal fault, from Glurns to the Piz Rims klippe. $P_{1'}$ and $P_{2'}$ are the intersection points of the Ötztal basal thrust with the Schlinig fault in the footwall and in the hangingwall, respectively, projected into the cross-section. The projection of $P_{1'}$ is not well constrained because the Piz Lad thrust is not planar. The intersection point in the cross-section must, however, be located northwest of the Piz Rims klippe because at Piz Rims, the base of the Ötztal rocks is still the cataclastic top-southeast normal fault, and there are no remnants of an older top-west thrust. Hence, the offset of the Ötztal basal thrust across the Schlinig fault measured parallel to the movement direction amounts to about 17 km (Fig. 6).

3.5. Initiation angle

As stated above, the present average dip angle of the Schlinig fault parallel to the movement direction is 7.5°, measured between Clusio/Schleis and the Piz Rims klippe (Fig. 6). Was the Schlinig fault initiated as a low-angle normal fault, or was it only later rotated into its present shallow orientation? An estimate of the initiation angle can be made using the variation in peak metamorphic temperatures across the footwall, provided that (1) these temperatures reflect the thermal state immediately preceding extensional faulting, (2) the preextensional geothermal gradient is known, and (3) the isotherms were horizontal prior to normal faulting (Wernicke, 1995).

For the footwall of the Schlinig fault, palaeotemperature data exist from petrologic and geochronological work of Thöni (1980b, 1981), and from combined illite crystallinity/vitrinite reflectance studies of Kürmann (1993) and Henrichs (1993). Ötztal gneiss above the Schlinig fault yielded undisturbed Variscan K–Ar biotite ages, whereas biotite in the footwall basement was partly rejuvenated during Cretaceous metamorphism (Thöni, 1980a,b). Hence, the Schlinig fault emplaced colder on hotter rocks and is discordant with respect to the temperature zonation. Therefore the temperature peak of Cretaceous metamorphism in the footwall (S-charl nappe) must have predated normal faulting along the Schlinig fault. On the other hand, the footwall did not cool down significantly before the normal faulting event, because microstructures in Schlinig mylonites and cataclasites (see above) indicate synfaulting temperatures that were still near the peak metamorphic temperatures. Therefore, the temperature data from the footwall can be taken as representing the thermal state immediately before normal faulting. For the southern S-charl nappe, Kürmann (1993) estimated a geotherm of 35 ± 5°C/km from illite crystallinity/vitrinite reflectance determinations at different structural depths. Henrichs (1993), using the same method, found geotherms of 40°C/km for the western S-charl nappe and 43°C/km for the southeastern S-charl nappe. For Cretaceous metamorphism in the southwestern Ötztal nappe, Schmid and Haas (1989) inferred conditions of ca. 440°C and 4 kbar for the chloritoid-in boundary. Assuming a density of 2.7 g/cm^3, this corresponds to a geotherm of 29.7°C/km. From these estimates, a gradient between 30°C/km and 45°C/km seems realistic. We chose 30° for the construction in Fig. 6. Assuming a higher geotherm would result in a lower initiation angle. The assumption that the isotherms in the S-charl nappe were about horizontal prior to exhumation appears reasonable because no Late Cre-

taceous igneous intrusions are known that could have complicated the thermal structure.

The distribution of palaeotemperatures estimated from combined illite crystallinity and vitrinite reflectance by Kürmann (1993) and Henrichs (1993) shows a temperature increase towards southeast within the S-charl nappe, indicative of a post-metamorphic northwest-side-down rotation of the nappe. Three of the sample localities lie on the profile of Fig. 6. The temperature at locality Schleis is above 300°C from IC/VR (Kürmann, 1993). From the mineral paragenesis and the results of radiometric dating, Thöni (1980b)) concluded that the temperature in this area was 'around 350°C but not much higher'. We assume 350°C for the locality Schleis. The temperature distribution fits a 30°C/km geotherm if the isograds are drawn with a northwesterly dip of 5° (Fig. 6). Hence, 5° is the rotation we can assume for the footwall. This implies that the initiation angle of the Schlinig fault was 7.5° (present dip angle between Piz Rims and Schleis) + 5° (rotation) = 12.5°. Hence, field relations suggest that the Schlinig fault represents a low-angle normal fault which was initiated at a shallow angle of 10° to 15° and was rotated only moderately during or after its activity.

3.6. Relation between shortening and extension in the footwall of the schlinig fault

The Upper Triassic Hauptdolomit of the S-charl nappe, in the footwall of the Schlinig fault, was severely stretched in a northwest–southeast direction (Schmid and Haas, 1989). The Hauptdolomit represents a carbonate platform of Norian age. It is embedded between two potential décollement horizons, the evaporite-bearing Raibl Formation of Carnian age below, and calcareous and shaly Jurassic to Cretaceous formations above. In the southeastern S-charl nappe, the Hauptdolomit is present as a layer of northwest-side-down tilted 'domino' blocks separated by southeast-dipping normal faults (Fig. 4b, c). This layer of tilted Hauptdolomit blocks ('S-charl Oberbau') is decoupled from the lower part of the Triassic sediments and the basement ('S-charl Unterbau') along the Raibl formation. As demonstrated by Schmid and Haas (1989), the importance of the normal faults dissecting the Hauptdolomit diminishes northwestward. In the northwest part of the S-charl nappe, the normal faults are absent and instead, northwest-directed thrust faults and northwest-facing folds with NE-striking axes deform the Hauptdolomit layer. Similarly oriented folds also occur in the 'S-charl Unterbau'.

These relations were interpreted by Schmid and Haas (1989) to indicate simultaneous folding/thrusting and normal faulting. According to these authors, the stretching reflects forced extrusion of the Hauptdolomit layer from below the westward advancing Ötztal nappe during Cretaceous thrusting. The same mechanism was proposed by Froitzheim (1988) to explain Alpine domino-style extension of Hauptdolomit in the Ortler nappe. Our new findings along the Schlinig fault, however, allow a different interpretation, namely, that the stretching of the Hauptdolomit layer postdates the folding and thrusting, and reflects extension in the footwall of and related to the Schlinig normal fault. As a third alternative, the stretching of the Hauptdolomit in the S-charl nappe might not be related to Alpine tectonics at all, but to Jurassic rifting (evidence for Jurassic rifting in the S-charl nappe was found by Mader, 1987). To test these alternatives, we retrodeformed the stretching of the Hauptdolomit using the cross-section by Schmid and Haas (1989) oriented parallel to the slip direction of the normal faults (Fig. 4c, Fig. 10). Retrodeformation was done by fitting the Hauptdolomit blocks together. Two generations of normal faults exist (Schmid and Haas, 1989). We first retrodeformed the younger and then the older generation. The retrodeformation is completely constrained by the geometry of the tilted-block layer.

The shape of the retrodeformed Hauptdolomit corresponds to an anticline (Fig. 10). This directly results from the keystone-like shape of the dominos which are wider at the top than at the base. The anticline may be interpreted as a fault-bend anticline related to a thrust underneath. The most important result of this retrodeformation is that the normal faults did not form simultaneously with the folds nor before the folds, but that they postdate folding. The amount of extension of the Hauptdolomit layer can be directly read from Fig. 10 (distance A′–B′ minus distance A–B). It is 7.85 km, corresponding to a stretch $1 + e$ of 2.67 (A′–B′ divided by A–B). This is in the range of what Schmid and Haas (1989) calculated ($1 + e = 3.45$) with a different

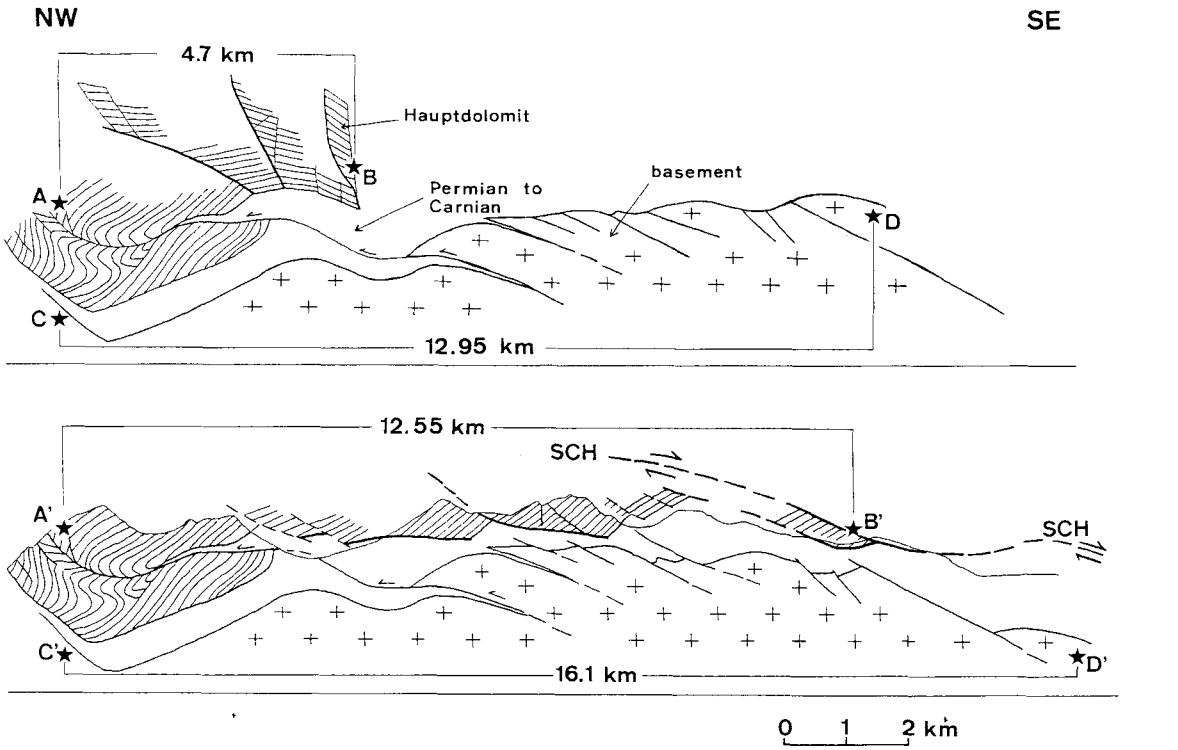

Fig. 10. Retrodeformation of domino-style extension in the footwall of the Schlinig fault. Lower section is taken from Schmid and Haas (1989) and is identical to Fig. 4c. Upper section shows pre-normal-faulting situation, restored by fitting the fault blocks together. *SCH* = Schlinig fault. *A, B, C* etc. are reference points. For further explanation, see text.

method, using the angular relationships of faults and bedding planes. Minor normal faulting also affected the 'S-charl Unterbau'. Extension of the 'Unterbau' amounts to 3.15 km (C'–D' minus C–D). Hence, the Hauptdolomit was extended by 7.85 km, and the 'Unterbau' only by 3.15 km. The difference is 4.7 km. This extra extension of the Hauptdolomit must have been transferred to deeper crustal levels along the Schlinig normal fault (if we do not assume rootless extension of the Hauptdolomit, e.g., by gravitational gliding, for which we do not see any evidence). Therefore, extension of the Hauptdolomit was kinematically linked to normal faulting along the Schlinig fault.

To conclude, we assume that the NW–SE extension of the Hauptdolomit layer postdates nappe imbrication and formation of NW-facing folds, and is kinematically linked with the Schlinig normal fault. The rotation of the Hauptdolomit blocks is antithetic (NW-side-down) with respect to the Schlinig fault, and is compatible with top-SE shear of the Hauptdolomit layer (compare fig. 6 in Schmid and Haas, 1989), with the domino-normal faults acting in a similar way as synthetic Riedel shears or shear bands in a mylonite.

4. Discussion

4.1. Reconstruction of pre-normal fault geometry

An attempt at restoring the geometry of the nappe stack before extensional faulting is made in Fig. 11. The cross-section used is the one of Fig. 6. Fig. 11a is the restored section. We assumed an initiation angle of 15° for the Schlinig fault, in accordance with the field relations (see above). The basal thrust of the Ötztal nappe is used as a reference level for the reconstruction. The Arlui fault is projected into the section from the north. In the reconstructed section, it joins the Schlinig fault at the point where the

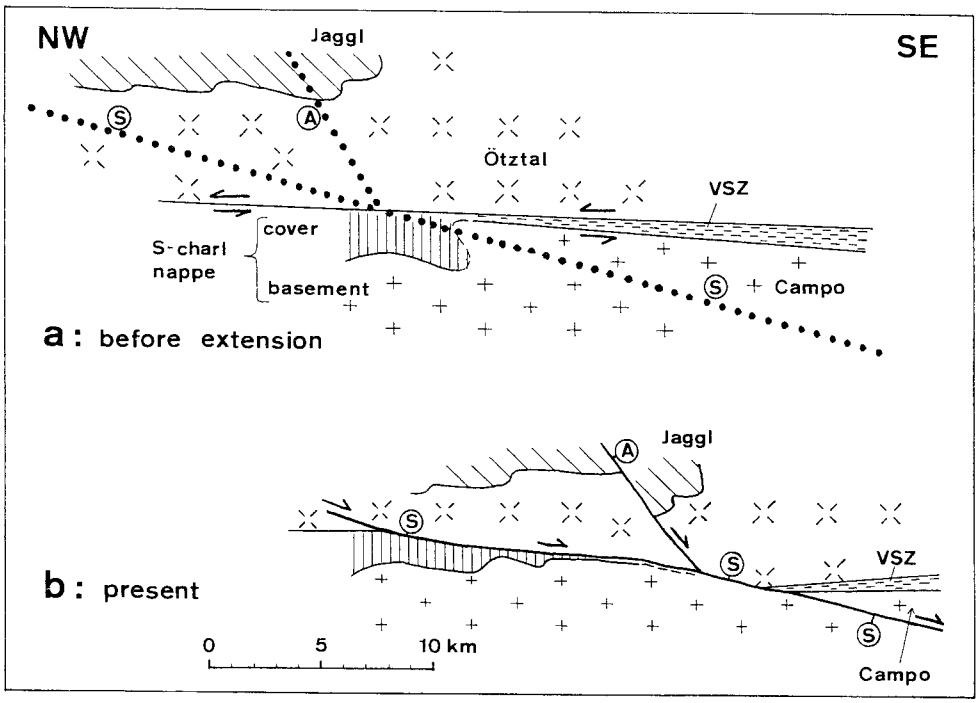

Fig. 11. Reconstruction of the Schlinig fault. (a) Pre-normal-faulting geometry of the Cretaceous nappe stack. Stippled lines are trajectories of future normal faults. (b) Present-day situation after normal faulting along the Schlinig and Arlui faults. *A* = Arlui fault; *S* = Schlinig fault; *VSZ* = Vinschgau shear zone.

latter passes through the Ötztal basal thrust. Two large thrust sheets exist in the reconstructed section, the lower S-charl-Campo thrust sheet (including the Ortler nappe south of the section) and the higher Ötztal thrust sheet (including the Umbrail–Chavalatsch zone and the Quattervals nappe). These were dissected by the Schlinig–Gallo fault. The S-charl–Campo thrust sheet was divided into a part in the hanging wall of the Schlinig–Gallo fault (Campo nappe, Ortler nappe) and a part in the footwall (S-charl nappe). The reconstruction shows some features that we regard as typical for the Late Cretaceous collapse in the western Austroalpine. The normal faults have a similar orientation as the earlier thrusts, only that they are often slightly steeper and the slip sense is reversed. They partly reactivate earlier thrusts, as was observed along the base of the Silvretta nappe (Froitzheim et al., 1994), but partly follow new trajectories at small angles to the thrusts. The extension is strongly asymmetric, to such a degree that antithetic, northwest-dipping normal faults are hardly ever observed.

4.2. Age of normal faulting

The Schlinig–Gallo fault system overprints older Alpine structures, mainly thrust faults and open to isoclinal folds. These older structures are attributed to the west- to northwestward imbrication of the Austroalpine nappe stack during the Late Cretaceous Trupchun phase. Trupchun-phase mylonites with top-west to top-northwest shear sense are abundant in the Umbrail–Chavalatsch Schuppenzone and in the Ortler nappe south of the Gallo line (Conti, 1994; Fig. 5). In the footwall of the Gallo–Schlinig fault system, they are largely overprinted by top-ESE shear due to normal faulting (Fig. 5). On the other hand, the Schlinig and Gallo normal faults are themselves slightly folded around ESE-striking axes, leading to anti- and synforms on the regional scale (Fig. 2), and to the quartz microfabrics described above on the microscopic scale. These folds are assigned to the Early Tertiary Blaisun phase. The normal faulting along the Schlinig and Gallo faults can therefore be attributed to the Ducan-Ela

extensional phase as defined in the area west of the Engadine line. We will briefly summarize the age constraints for the Ducan-Ela phase in order to discuss the large-scale tectonic scenario.

The youngest sediments in the Engadine dolomites are Cenomanian to possibly middle Turonian foraminiferal marls in the core of a Trupchun-phase syncline at the western end of the Ortler nappe (Caron et al., 1982). Trupchun-phase thrusting and folding in this area can therefore only have begun after about 93.5 Ma (age of the Cenomanian–Turonian boundary after Gradstein et al., 1994). On the other hand, the youngest fossils found in Penninic units of the Engadine window, underlying the Austroalpine nappes, are Paleocene to Lower Eocene Formanifera found in a flysch unit in the western part of the window (Ziegler, 1956; Rudolph, 1982; Eiermann, 1988). Hence the thrusting of the Austroalpine nappes en bloc over the Penninic units of the window, occurred soon after 50 Ma. Overprinting relations (see above and Froitzheim et al., 1994) show that this thrusting postdates the Ducan extension. Therefore, from biostratigraphic evidence, Trupchun-phase thrusting and subsequent normal faulting along the Schlinig–Gallo fault system occurred between 93.5 and 50 Ma.

Radiometric data further constrain the timing. Dating of extension-related pseudotachylyte in the Silvretta nappe (79–73 Ma using Rb–Sr, Thöni, 1988) and of mica grown along Ducan-Ela-phase cleavage in the Lower Austroalpine (80–67 Ma using K–Ar, Tietz et al., 1993) suggest that the Ducan-Ela extensional phase in the western Austroalpine realm lasted from about 80 Ma to 67 Ma, with some uncertainty due to the scarcity of data. Alpine metamorphism in the Engadine dolomites, Campo nappe, and Ötztal nappe was radiometrically dated by Thöni and coworkers (Thöni, 1980b, 1981, 1986, 1988; Thöni and Miller, 1987, reviewed in Schmid and Haas, 1989). Virtually all the ages from the study area are between 100 and 70 Ma. These include both formation ages and cooling ages. K/Ar ages from fine-grained muscovite/phengite in the southeastern S-charl nappe clustering around 80 ± 6 Ma are interpreted as cooling ages, whereas ages from the northeastern S-charl nappe around 90 ± 5 Ma are interpreted as formation ages (Thöni, 1980b). The cooling ages approximately coincide with the assumed age of the Ducan-Ela extensional phase, which suggests that cooling was related to extensional exhumation.

4.3. In search of a tectonic model for Late Cretaceous extension

A Late Cretaceous extensional overprint has been demonstrated in many areas of the Austroalpine realm. Prior to the present study, such extensional faulting was already reported by Krohe (1987), Ratschbacher et al. (1989), Froitzheim (1992), Werling (1992), Froitzheim et al. (1994), Neubauer et al. (1995), Fügenschuh (1995), and several others. The extensional faults and shear zones identified by these authors generally overprint earlier thrust faults, have a transport direction towards east (NE to SE), and have important displacements, often in the range of tens of kilometres. In many areas, but not generally (see Krohe, 1987), the transport direction is opposite to the direction of earlier thrusting.

4.3.1. Late Cretaceous extension and the Gosau basins

According to Krohe (1987), Ratschbacher et al. (1989) and Neubauer et al. (1995), Late Cretaceous normal faulting is related to the formation of basins in which sediments of the Gosau Group were deposited. The Gosau Group is of late Turonian to Early Eocene age (90 to 50 Ma) in the Northern Calcareous Alps and of Santonian to Maastrichtian age (86 to 65 Ma) in the Central Austroalpine basement east of the Tauern window (Wagreich, 1995; Neubauer et al., 1995). The Lower Gosau Subgroup (Wagreich and Faupl, 1994) rests unconformably on folded and imbricated older rocks and comprises fluviatile (at the base) to shallow marine (at the top) sediments deposited in small, fault-bounded basins (Wagreich, 1995). The Upper Gosau Complex comprises deep-sea fan facies, deposited partly below the CCD, and marly slope facies, and was not restricted to single basins but covered the entire Northern Calcareous Alps (Wagreich, 1995). The boundary between the Lower and Upper Complex is related to a major subsidence pulse that occurred diachronously, between late Turonian/Santonian (90 to 83.5 Ma) and Maastrichtian (71 to 65 Ma) (Wagreich, 1995). The correlation between Late Cretaceous normal faulting

and Gosau basin formation is well established for the Gosau basins located in the Central Austroalpine basement east of the Tauern window (Neubauer et al., 1995), and is also probable for the Northern Calcareous Alps because Ortner (1994) and Eisbacher and Brandner (1996) demonstrated that Gosau sediments of the western Northern Calcareous Alps seal SW–NE-trending folds (= Trupchun phase) and are themselves deformed by WNW–ESE-trending folds (= Blaisun phase).

4.3.2. Relation between extension and strike-slip faulting

Neubauer et al. (1995) demonstrated that in the Central Austroalpine area east of the Tauern window (Fig. 1), Late Cretaceous extensional shearing and Gosau basin formation were coeval with sinistral strike-slip along E–W- to NE–SW-striking shear zones. On the other hand, Ortner (1994) and Eisbacher and Brandner (1996) demonstrated that formation of Gosau basins in the Northern Calcareous Alps (Fig. 1) was related to *dextral* slip along faults that presently trend SE–NW but trended E–W during the Late Cretaceous (fig. 4 of Eisbacher and Brandner, 1996). Therefore, the extension was apparently associated with sinistral strike-slip in the more southerly located Central Austroalpine, and with dextral strike-slip to the north, in the NCA.

4.3.3. Contemporaneity of extension and subduction

In the western Austroalpine, the extensional phase is coeval with subduction of Piemont–Ligurian oceanic lithosphere and continental slivers below the Austroalpine continental crust. As discussed in Froitzheim et al. (1996), the Sesia zone in the Western Alps (Fig. 1, inset) probably represents a continental sliver in the Piemont–Ligurian oceanic basin, near the Apulian (Austroalpine–South Alpine) continental margin. The widespread eclogite facies metamorphism of the Sesia zone (Compagnoni et al., 1977) developed when this continental sliver was subducted under the Apulian margin. Recent geochronological studies (Ramsbotham et al., 1994; Rubatto et al., 1995) indicate that peak pressures were reached at or shortly before 65 Ma. Hence the Sesia rocks must have been on their way down the subduction zone at the same time when the Austroalpine crust in the upper plate was severely stretched in an east–west direction (80–67 Ma). On the other hand, the Late Cretaceous extension postdates older Cretaceous eclogite metamorphism *within* the Austroalpine nappes. These older eclogites formed during collision after the closure of the Meliata–Hallstatt ocean, remnants of which are found in the eastern NCA (Fig. 1, inset). The exhumation of these eclogites was at least partly accommodated by the Late Cretaceous extension (Neubauer, 1994; Froitzheim et al., 1996). The contemporaneity of extension in the Austroalpine realm and subduction along the southeastern margin of the Piemont–Ligurian ocean puts an important constraint on the tectonic model: Late Cretaceous extension occurred in the upper plate of an active subduction zone.

A model for Late Cretaceous extension of the Austroalpine region is constrained by the following observations: (1) regional subsidence to below-CCD depth concomitant with extension; (2) connection of east–west-directed extension with dextral strike-slip in the north and sinistral strike-slip in the south; (3) contemporaneity of extension with subduction along the Austroalpine–Penninic boundary. Regional extension of previously thickened crust in orogenic belts is caused by a change in the stress regime within this crust from deviatoric compression to deviatoric tension. Several models have been put forward to explain this (Fig. 12). In models of Fig. 12a–d (left side), extension is driven by locally generated forces associated with topography. In the orogenic wedge model (Platt, 1986; Fig. 12a) extension occurs when the surface slope of the wedge exceeds a dynamically stable configuration, for example, due to underplating of material at the base of the wedge. A decrease or cessation of plate convergence may also lead to a decrease of horizontal normal stress in the orogen and hence to a change from deviatoric compression to tension (Fig. 12b; see Molnar and Lyon-Caen, 1988). Convective removal of lithosphere (Fig. 12c; Fleitout and Froidevaux, 1982; Platt and England, 1994) and slab breakoff (Fig. 12d; Wortel and Spakman, 1992; von Blanckenburg and Davies, 1995, 1996) both lead to a rapid increase in surface elevation which may result in extension of the orogen. Models where the extension is mainly driven by forces created outside the extending area are sketched on the right side of Fig. 12 (e–g):

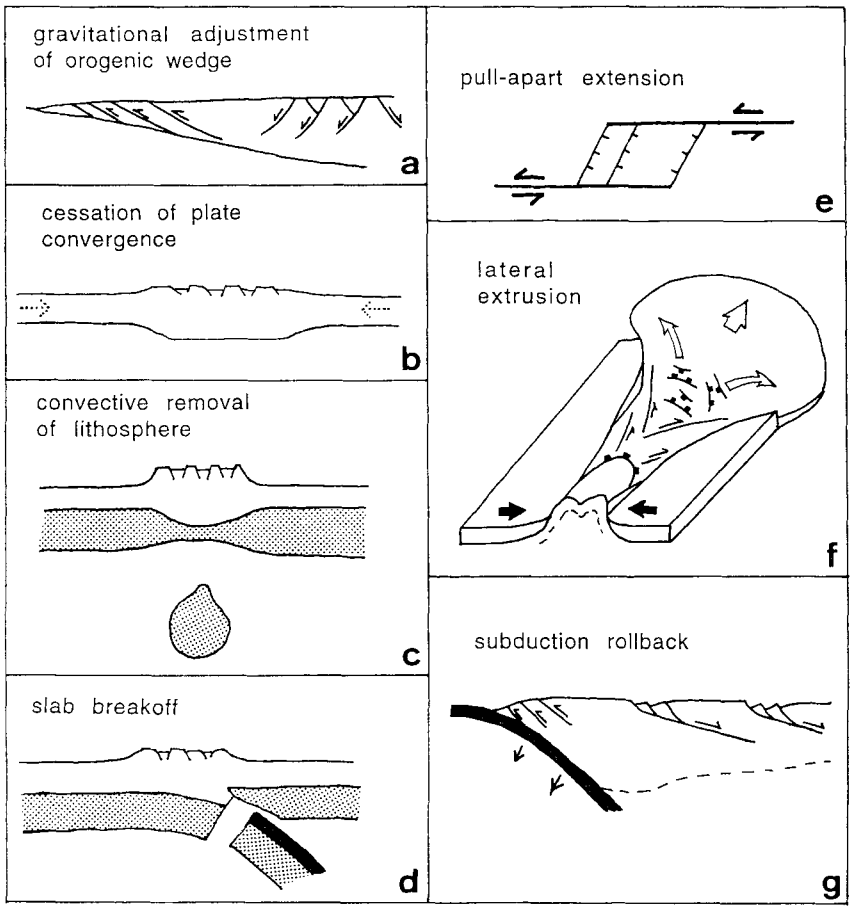

Fig. 12. Different models explaining regional extension in orogens. (a) Gravitational adjustment of an unstable orogenic wedge (after Platt, 1986). (b) Cessation of plate convergence. (c) Convective removal of lithospheric root (after Fleitout and Froidevaux, 1982). (d) Slab breakoff (after von Blanckenburg and Davies, 1996, slightly modified). (e) Pull-apart extension. (f) Lateral extrusion from a collision zone (after Ratschbacher et al., 1989, 1991. Note that this model was designed for Miocene, not Cretaceous, extension in the Eastern Alps). (g) Subduction rollback (after Hetzel et al., 1995). Stippled represents mantle lithosphere, black is oceanic crust.

pull-apart extension in a strike-slip regime, lateral extrusion from a collision zone (Ratschbacher et al., 1991), and subduction rollback (Royden and Burchfiel, 1989).

Gravitational adjustment of an unstable orogenic wedge (Fig. 12a; Platt, 1986), was proposed by Ratschbacher et al. (1989) and Froitzheim et al. (1994) to explain Late Cretaceous extension in the Austroalpine realm. More specifically, Ratschbacher et al. (1989) assumed that the extension was caused by underplating of the buoyant 'Zentralgneiss terrane' exposed in the Tauern window of the Eastern Alps (Fig. 1, inset). The model appears unlikely for two reasons. Firstly, gravitational adjustment tends to keep the surface slope in the orogenic wedge constant in order to maintain the dynamically stable configuration (Platt, 1986). This process can therefore hardly explain the subsidence of the surface of the orogenic wedge to below the CCD, as observed during extension in the Austroalpine realm. Secondly, underplating of the Zentralgneiss terrane postdated the Late Cretaceous extension of the Austroalpine nappes (Kurz et al., 1996). A cessation or significant decrease of plate convergence (Fig. 12b) may be ruled out as well because contemporaneous eclogitization of Sesia rocks (see above) indicates ongoing convergence. Convective removal of lithosphere (Fig. 12c) or slab breakoff (Fig. 12d) may

have occurred in the Cretaceous Alps (von Blanckenburg and Davies, 1996), but we doubt that these mechanisms have caused the extension. In both models, extension is mainly the result of a rapid increase in surface elevation, leading to a high mountain chain or plateau (Platt and England, 1994; von Blanckenburg and Davies, 1996). The absence of volumetrically significant molasse-type sediments of Cretaceous age within the Austroalpine and in the neighbouring areas makes the existence of such a high range unlikely. During the Cretaceous period, the Austroalpine area represented a sea with temporarily emergent highs rather than a high mountain range (see palaeogeographic maps in Oberhauser, 1995).

Neubauer et al. (1995) proposed that Late Cretaceous extension in the eastern part of the Austroalpine nappes resulted from a releasing bend in an east–west-trending sinistral wrench corridor (Fig. 12c). This cannot serve as a general explanation for Late Cretaceous extension, since extension is connected with dextral strike-slip along east–west faults in other parts of the Austroalpine region (see above). Lateral extrusion from a collision area (Fig. 12f) is unlikely as well because Late Cretaceous extension in the Austroalpine region occurred before the continental collision between Europe and the Austroalpine region, when the Piemont–Liguria ocean was still open (e.g., Neubauer, 1994; Froitzheim et al., 1996).

4.3.4. Late Cretaceous subduction rollback in the Piemont–Liguria ocean

Royden and Burchfiel (1989) and Royden (1993) proposed that systematic variations in the style of thrust belts in the Alpine system resulted from different ratios between the rate of subduction and the rate of plate convergence. Contemporaneous subduction and back-arc extension occur when the rate of subduction of one plate is greater than the rate of overall plate convergence. This results in oceanward retreat of the subduction boundary (subduction rollback, Fig. 12g). Royden (1993) assumed that this process can affect limited segments of a subduction boundary while other segments of the same boundary remain stationary (with respect to a point in the interior of the upper plate) which leads to the formation of strongly arcuate segments retreating into the ocean, bounded by strike-slip zones on both sides. The driving force of the rollback is gravity acting on a dense subducting slab (Royden, 1993). We propose that this model applies to the Late Cretaceous extension of the Austroalpine area (Fig. 13). The marginal, southeastern part of the Piemont–Ligurian oceanic lithosphere which was subducted under the Austroalpine–South Alpine margin during the Late Cretaceous (probably beginning at about 100 to 90 Ma, see discussion in Froitzheim et al., 1996), was in fact dense. It was old (formed since about 165 Ma) and devoid of a well-developed crustal section, because it had been formed by extensional denudation of subcontinental mantle (Lemoine et al., 1987; Froitzheim and Manatschal, 1996). The contemporaneity of the extension with subduction along the plate boundary (see above) strongly favours this model. Furthermore, we can explain the association of extensional structures with dextral strike-slip in the north (Northern Calcareous Alps) and with sinistral strike-slip in the south (Central Austroalpine). These two strike-slip systems accommodated the westward retreat of a small segment of the subduction boundary (Fig. 13c). Typical for a subduction rollback scenario is also the low topographic elevation (Royden, 1993) of the Austroalpine area in the Late Cretaceous, below sea level for the most part.

The assumed westward retreat of the subduction boundary in the Late Cretaceous would also explain why Late Cretaceous east–west extension is ubiquitous in the Austroalpine nappes but absent in the Southern Alps: the Southern Alps were located south of the sinistral strike-slip fault delimiting the westward retreating segment of the subduction boundary. This assumption implies that the dextrally transpressive, Tertiary-age Insubric line (Fig. 1), forming the limit between Austroalpine and Southern Alps, had a sinistral forerunner in the Late Cretaceous (palaeo-Insubric line in Fig. 13c). In fact, there is some structural evidence that Late Cretaceous sinistral strike-slip zones exist adjacent to the Periadriatic fault in the Eastern Alps (Unzog, 1989).

After the stage sketched in Fig. 13b and c, the main direction of convergence between the Austroalpine area and Europe changed from E–W to N–S. In this new kinematic framework, the closure of the Piemont–Ligurian ocean and continental col-

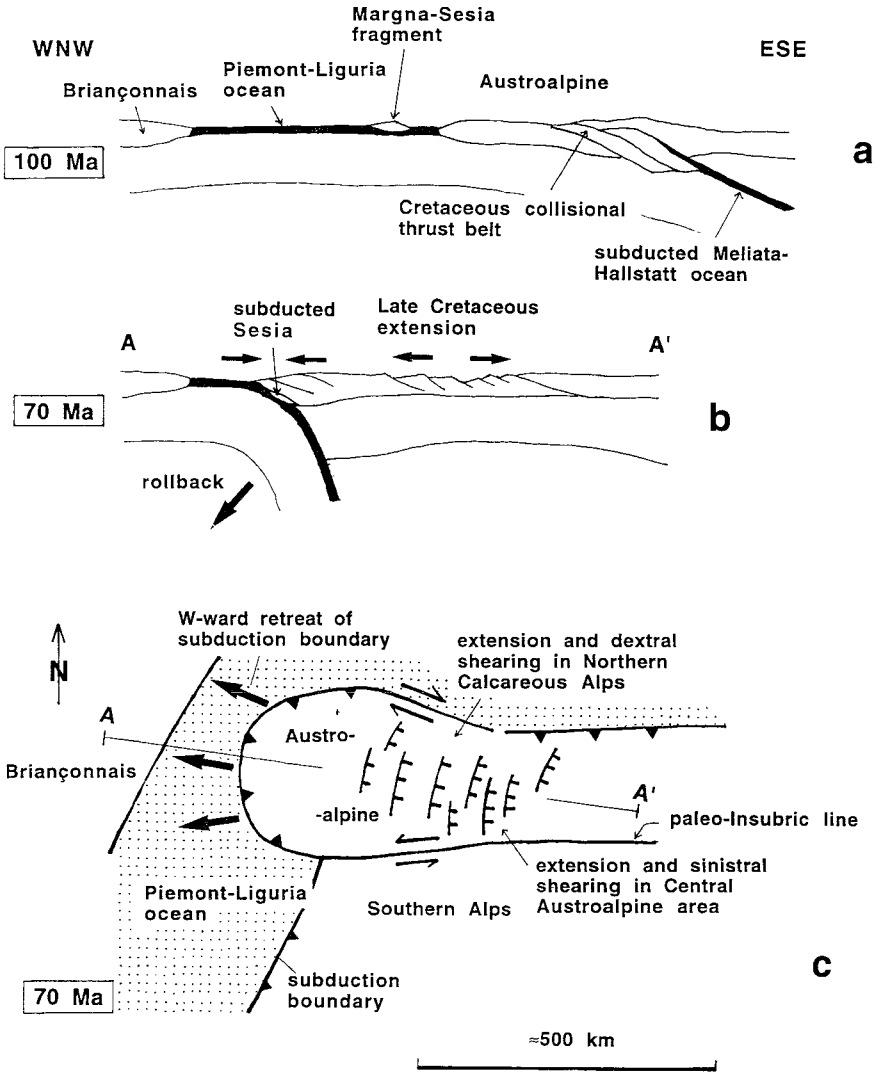

Fig. 13. Hypothetical large-scale scenario for the Late Cretaceous evolution of the Austroalpine nappes. (a) Situation at 100 Ma (Trupchun phase). Crustal stacking within the Austroalpine realm results from footwall propagation of thrusting after continental collision along the Meliata–Hallstatt suture. Subduction of Piemont–Ligurian oceanic lithosphere is just about to begin. (b) Situation at 70 Ma (Ducan-Ela phase). Piemont–Ligurian lithosphere is being subducted at a rate higher than the overall plate convergence, leading to oceanward retreat of the subduction boundary and extension of the Austroalpine upper plate by ESE-dipping normal faults, contemporaneous with subduction of the Sesia zone to eclogite-facies depth. (c) Map view of the situation at 70 Ma. Westward retreat of the subduction boundary is restricted to the Austroalpine segment of this boundary and is accommodated by a sinistral shear zone to the south ('palaeo-Insubric line') and a dextral shear zone to the north.

lision (= Blaisun phase) took place in the Paleocene to Eocene. Finally, Late Oligocene to Miocene NW–SE-convergence led to a reversal of the shear sense along the Insubric line which then accommodated dextral strike-slip and south-directed backthrusting (Schmid et al., 1987).

5. Conclusions

The Schlinig fault is a Late Cretaceous normal fault overprinting a stack of thrust sheets imbricated slightly earlier, also during the Late Cretaceous. The slip direction of the normal fault is SE to ESE,

and the displacement in this direction amounted to about 17 km. The present dip angle of the fault, measured parallel to the slip direction, is between 5° and 10°. The initial dip angle of the fault was less than 20°. Hence, the Schlinig fault represents a low-angle normal fault. Although apparently at variance with Andersonian fault mechanics and the seismic record (Jackson, 1987), existence of such low-angle normal faults is indicated by an increasing body of field evidence (e.g. John and Foster, 1993; Wernicke, 1995) to which the present study adds.

Shape fabric and crystallographic preferred orientation in dynamically recrystallized quartz layers of a Schlinig mylonite record two subsequent deformation events, first the top-ESE shear related to Late Cretaceous normal faulting, and second, shortening in the NNE–SSW direction related to Early Tertiary collisional deformation. The same sequence of events is reflected by large-scale, open folding of the normal fault around ESE-trending axes. Domino-style extension of the competent Hauptdolomit layer in the footwall of the Schlinig fault was kinematically linked with normal slip along the fault itself. Extrusion models which assume domino extension to be caused by thrusting do not apply in this case.

Late Cretaceous extensional deformation in the Austroalpine realm accommodated the formation of the Gosau basins, was associated with sinistral strike-slip in the south (Central Austroalpine) and with dextral strike-slip in the north (Northern Calcareous Alps), and was coeval with subduction along the Austroalpine–Penninic boundary. Westward retreat (rollback) of a part of this subduction boundary is proposed to have caused the extension. ~~Not referred to: Dal Piaz et al., 1988; Eiermann, 1988; von Blanckenburg, 1992; Ziegler, 1956~~

Acknowledgements

We thank S. Schmid and H. Stünitz for stimulating discussions, F. Neubauer and F. v. Blanckenburg for very constructive reviews, and M. Thöni and B. Fügenschuh for some interesting remarks. Supported by Swiss National Science Foundation grants No. 21-25252.88 and 20-29869.90 (N. Froitzheim and P. Conti) and No. 21-36008.92 and 20-42134.94 (M. van Daalen).

References

Avé Lallemant, H.J. and Carter, N.L., 1971. Pressure dependence of quartz deformation lamellae orientations. Am. J. Sci, 270: 218–235.

Böse, E., 1896. Zur Kenntnis der Schichtenfolge im Engadin. Z. Dtsch. Geol. Ges., 48: 557–631.

Caron, M., Dössegger, R., Steiger, R. and Trümpy, R., 1982. Das Alter der jüngsten Sedimente der Ortler-Decke (Oberostalpin) in der Val Trupchun (Schweizerischer Nationalpark, Graubünden). Eclogae Geol. Helv., 75: 159–169.

Carter, N.L., Christie, J.M. and Griggs, D.T., 1964. Experimental deformation and recrystallization of quartz. J. Geol., 72: 687–733.

Compagnoni, R., Dal Piaz, G.V., Hunziker, J.C., Gosso, G., Lombardo, B. and Williams, P.F., 1977. The Sesia–Lanzo zone, a slice of continental crust with Alpine high pressure–low temperature assemblages in the western Italian Alps. Rend. Soc. Ital. Mineral. Petrol., 33(1): 281–334.

Conti, P., 1992. Tettonica delle falde Austroalpine nelle Dolomiti dell'Engadina: un'ipotesi di lavoro. Atti Ticinensi Sci. Terra, 35: 61–64.

Conti, P., 1994. La Falda dell'Ortles: struttura interna e suo ruolo nell'evoluzione tettonica delle Dolomiti dell'Engadina (Prov. Sondrio, Bolzano e Cantone dei Grigioni). Ph.D. thesis, Universität Basel, Basel, 163 pp.

Conti, P., Manatschal, G. and Pfister, M., 1994. Synrift sedimentation, Jurassic and Alpine tectonics in the central Ortler nappe (Eastern Alps, Italy). Eclogae Geol. Helv., 87: 63–90.

Dal Piaz, G.V., Del Moro, A., Martin, S. and Venturelli, G., 1988. Post-collisional magmatism in the Ortler–Cevedale Massif (Northern Italy). Jahrb. Geol. Bundesanst. Wien, 131: 533–551.

Drury, M.R., 1993. Deformation lamellae in metals and minerals. In: J.N. Boland and J.D. Fitz Gerald (Editors), Defects and Processes in the Solid State: Geoscience Applications. The McLaren Volume, Elsevier, Amsterdam, pp. 195–212.

Drury, M.R. and Urai, J.L., 1990. Deformation-related recrystallization processes. Tectonophysics, 172: 235–253.

Eiermann, D.R., 1988. Zur Stellung des Martegnas-Zuges. Eclogae Geol. Helv., 81: 259–272.

Eisbacher, G.H. and Brandner, R., 1996. Superposed fold-thrust structures and high-angle faults, Northwestern Calcareous Alps, Austria. Eclogae Geol. Helv., 89: 553–571.

Fleitout, L. and Froidevaux, C., 1982. Tectonics and topography for a lithosphere containing density heterogeneities. Tectonics, 1: 21–56.

Froitzheim, N., 1988. Synsedimentary and synorogenic normal faults within a thrust sheet of the Eastern Alps (Ortler zone, Graubünden, Switzerland). Eclogae Geol. Helv., 81: 593–610.

Froitzheim, N., 1992. Formation of recumbent folds during synorogenic crustal extension (Austroalpine nappes, Switzerland). Geology, 20: 923–926.

Froitzheim, N. and Manatschal, G., 1996. Kinematics of Jurassic rifting, mantle exhumation, and passive-margin formation in the Austroalpine and Penninic nappes (Eastern Switzerland). Bull. Geol. Soc. Am., 108: 1120–1133.

Froitzheim, N., Schmid, S.M. and Conti, P., 1994. Repeated change from crustal shortening to orogen-parallel extension in the Austroalpine units of Graubünden. Eclogae Geol. Helv., 87: 559–612.

Froitzheim, N., Schmid, S.M. and Frey, M., 1996. Mesozoic paleogeography and the timing of eclogite-facies metamorphism in the Alps: a working hypothesis. Eclogae Geol. Helv., 89: 81–110.

Fügenschuh, B., 1995. Thermal and Kinematic History of the Brenner Area (Eastern Alps, Tyrol). Ph.D. thesis, ETH Zürich, Zürich, 225 pp.

Gradstein, F.M., Agterberg, F.P., Ogg, J.G., Hardenbol, J., van Veen, P., Thierry, J. and Huang, Z., 1994. A Mesozoic time scale. J. Geophys. Res., 99(B12): 24,051–24,074.

Guillopé, M. and Poirier, J.P., 1979. Dynamic recrystallization during creep of single-crystalline halite: an experimental study. J. Geophys. Res., 84: 5557–5567.

Hammer, W., 1908. Beiträge zur Geologie der Sesvennagruppe. Verh. K.K. Geol. Reichsanst., 4: 98–107.

Heim, A., 1922. Geologie der Schweiz, Band II. Die Schweizer Alpen. Tauchnitz, Leipzig, 1018 pp.

Henrichs, C., 1993. Sedimentpetrographische Untersuchungen zur Hochdiagenese in der Kössen-Formation (Obere Trias) der westlichen Ostalpen und angrenzender Südalpengebiete. Bochumer Geol. Geotech. Arb., 40: 1–206.

Hess, W., 1953. Beiträge zur Geologie der südöstlichen Engadiner Dolomiten zwischen dem oberen Münstertal und der Valle di Fraéle (Graubünden). Eclogae Geol. Helv., 46: 39–142.

Hess, W., 1962. Über den Jaggl (Cima del Termine) am Reschenpass (Passo di Resia), Südtirol, und seine Deutung. Eclogae Geol. Helv., 55: 407–416.

Hetzel, R., Passchier, C.W., Ring, U. and Dora, Ö.O., 1995. Bivergent extension in orogenic belts: the Menderes massif (southwestern Turkey). Geology, 23: 455–458.

Jackson, J.A., 1987. Active normal faulting and crustal extension. In: M.P. Coward, J.F. Dewey and P.L. Hancock (Editors), Continental Extensional Tectonics. Geol. Soc. London, Spec. Publ., 28: 3–17.

John, B.E. and Foster, D.A., 1993. Structural and thermal constraints on the initiation angle of detachment faulting in the southern Basin and Range: the Chemehuevi Mountains case study. Bull. Geol. Soc. Am., 105: 1091–1108.

Krohe, A., 1987. Kinematics of Cretaceous nappe tectonics in the Austroalpine basement of the Koralpe region (eastern Austria). Tectonophysics, 136: 171–196.

Kürmann, H., 1993. Zur Hochdiagenese und Anchimetamorphose in Permotrias-Sedimenten des Austroalpins westlich der Tauern. Bochumer Geol. Geotech. Arb., 41: 1–328.

Kurz, W., Neubauer, F., and Genser, J., 1996. Kinematics of Penninic nappes (Glockner Nappe and basement-cover nappes) in the Tauern Window (Eastern Alps, Austria) during subduction and Penninic–Austroalpine collision. Eclogae Geol. Helv., 89: 573–605.

Lemoine, M., Tricart, P. and Boillot, G., 1987. Ultramafic and gabbroic ocean floor of the Ligurian Tethys (Alps, Corsica, Apennines): in search of a genetic model. Geology, 15: 622–625.

Lister, G.S., 1977. Discussion: crossed-girdle *c*-axis fabrics in quartzites plastically deformed by plane strain and progressive simple shear. Tectonophysics, 39: 51–54.

Lister, G.S. and Snoke, A.W., 1984. S–C mylonites. J. Struct. Geol., 6: 617–638.

Lister, G.S. and Williams, P.F., 1979. Fabric development in shear zones: theoretical controls and observed phenomena. J. Struct. Geol., 1: 283–297.

Mader, P., 1987. Die Jura- und Kreideablagerungen im Lischana-Gebiet (Oberostalpine S-charl-Decke, Unterengadin). Eclogae Geol. Helv., 80: 633–653.

Molnar, P. and Lyon-Caen, H., 1988. Some simple aspects of the support, structure, and evolution of mountain belts. Geol. Soc. Am., Spec. Pap., 218: 179–207.

Neubauer, F., 1994. Kontinentkollision in den Ostalpen. Geowissenschaften, 12: 136–140.

Neubauer, F., Dallmeyer, R.D., Dunkl, I. and Schirnik, D., 1995. Late Cretaceous exhumation of the metamorphic Gleinalm dome, Eastern Alps: kinematics, cooling history and sedimentary response in a sinistral wrench corridor. Tectonophysics, 242: 79–98.

Oberhauser, R., 1995. Zur Kenntnis der Tektonik und der Paläogeographie des Ostalpenraumes zur Kreide-, Paleozän- und Eozänzeit. Jahrb. Geol. Bundesanst. Wien, 138: 369–432.

Ortner, H., 1994. Die Muttekopfgosau (Lechtaler Alpen, Tirol, Österreich): Sedimentologie und Beckenentwicklung. Geol. Rundsch., 83: 197–211.

Panozzo, R.H., 1983. Two-dimensional analysis of shape-fabric using projections of digitized lines in a plane. Tectonophysics, 95: 279–294.

Panozzo, R.H., 1984. Two-dimensional strain from the orientation of lines in a plane. J. Struct. Geol., 6: 215–221.

Passchier, C.W. and Simpson, C., 1986. Porphyroclast systems as kinematic indicators. J. Struct. Geol., 8: 831–843.

Platt, J.P., 1986. Dynamics of orogenic wedges and the uplift of high-pressure metamorphic rocks. Bull. Geol. Soc. Am., 97: 1037–1053.

Platt, J.P. and England, P.C., 1994. Convective removal of lithosphere beneath mountain belts: thermal and mechanical consequences. Am. J. Sci., 294: 307–336.

Ramsbotham, W., Inger, S., Cliff, B., Rex, D. and Barnicoat, A., 1994. Time constraints on the metamorphic and structural evolution of the southern Sesia–Lanzo Zone, Western Italian Alps. Mineral. Mag., 58A: 758–759.

Ratschbacher, L., Frisch, W., Neubauer, F., Schmid, S.M. and Neugebauer, J., 1989. Extension in compressional orogenic belts: the Eastern Alps. Geology, 17: 404–407.

Ratschbacher, L., Merle, O., Davy, P. and Cobbold, P., 1991. Lateral extrusion in the Eastern Alps, Part I. Boundary conditions and experiments scaled for gravity. Tectonics, 10: 245–256.

Royden, L.H., 1993. Evolution of retreating subduction boundaries formed during continental collision. Tectonics, 12: 629–638.

Royden, L. and Burchfiel, B.C., 1989. Are systematic variations

in thrust belt style related to plate boundary processes? (The Western Alps versus the Carpathians). Tectonics, 8: 51–61.

Rubatto, D., Gebauer, D., Compagnoni, R. and Sanchez-Rodriguez, L., 1995. A 65 Ma age for the eclogitization of continental crust at Monte Mucrone (Sesia–Lanzo Zone, Western Alps, Italy). International Workshop on Orogenic Lherzolites and Mantle Processes, Granada, 1995, Abstracts, pp. 56–57.

Rudolph, J., 1982. Tieferes Tertiär im oberen Fimbertal, Unterengadiner Fenster. Neues Jahrb. Geol. Paläontol. Monatsh., 1982/3: 181–183.

Sander, B., 1970. An Introduction to the Study of Fabrics of Geological Bodies. Pergamon Press, Oxford, 641 pp.

Schmid, S., 1973. Geologie des Umbrailgebiets. Eclogae Geol. Helv., 66: 101–210.

Schmid, S.M. and Casey, M., 1986. Complete fabric analysis of some commonly observed quartz *c*-axis patterns. Geophys. Monogr., 36: 263–286.

Schmid, S.M. and Froitzheim, N., 1993. Oblique slip and block rotation along the Engadine line. Eclogae Geol. Helv., 86: 569–593.

Schmid, S.M. and Haas, R., 1989. Transition from near-surface thrusting to intrabasement décollement, Schlinig thrust, eastern Alps. Tectonics, 8: 679–718.

Schmid, S.M., Zingg, A. and Handy, M., 1987. The kinematics of movements along the Insubric Line and the emplacement of the Ivrea Zone. Tectonophysics, 135: 47–66.

Spitz, A. and Dyhrenfurth, G., 1914. Monographie der Engadiner Dolomiten zwischen Schuls, Scanfs und dem Stilfserjoch. Beitr. Geol. Karte Schweiz, N.F., 44: 1–235.

Staub, R., 1937. Geologische Probleme um die Gebirge zwischen Engadin und Ortler. Denkschr. Schweiz. Naturforsch. Ges., 72: 1–115.

Stutz, E. and Walter, U., 1983. Zu Stratigraphie und Tektonik am Nordostrand der Engadiner Dolomiten am Schlinigpass (Gemeinden Sent, Graubünden und Mals, Südtirol). Eclogae Geol. Helv., 76: 523–550.

Thöni, M., 1973. Ein neues Sedimentvorkommen nahe dem Westrand des Ötztaler Altkristallins und einige Bemerkungen zur Deutung der Permotrias des Jaggl als Fenster. Verh. Geol. Bundesanst. Wien, 1973: 235–242.

Thöni, M., 1980a. Zur Westbewegung der Ötztaler Masse. Räumliche und zeitliche Fragen an der Schlinigüberschiebung. Mitt. Ges. Geol. Bergbaustud. Österr., 26: 247–275.

Thöni, M., 1980b. Distribution of pre-Alpine and Alpine metamorphism of the southern Ötztal mass and the Scarl unit, based on K/Ar age determinations. Mitt. Österr. Geol. Ges., 71/72: 139–165.

Thöni, M., 1981. Degree and evolution of the Alpine metamorphism in the Austroalpine unit W of the Hohe Tauern in the light of K/Ar and Rb/Sr age determinations on micas. Jahrb. Geol. Bundesanst. Wien, 124: 111–174.

Thöni, M., 1986. The Rb–Sr thin slab isochron method — an unreliable geochronologic method for dating geologic events in polymetamorphic terrains? Mem. Sci. Geol. Univ. Padova, 38: 283–352.

Thöni, M., 1988. Rb–Sr isotopic resetting in mylonites and pseudotachylytes: implications for the detachment and thrusting of the Austroalpine basement nappes in the Eastern Alps. Jahrb. Geol. Bundesanst. Wien, 131: 169–201.

Thöni, M. and Miller, J.A., 1987. ^{40}Ar–^{39}Ar and Rb–Sr results from the Austroalpine sheet (abstract). Terra Cognita, 7: 93.

Tietz, R., Handy, M.R., Villa, I. and Kamber, B., 1993. Strukturgeologische und radiometrische Untersuchungen an der Grenze Unterostalpin–Penninikum im Raume Piz Lunghin und Piz dal Sasc (GR). Schweizerisches Tektonikertreffen Zürich, 26–27 February 1993, Abstracts.

Torricelli, G., 1956. Geologie der Piz Lad–Piz Ajüz-Gruppe. Ph. D. thesis, Universität Bern, Bern, 83 pp.

Trümpy, R., 1980. Geology of Switzerland; A Guide-book. Wepf and Co., Basel, 334 pp.

Unzog, W., 1989. Schertektonik im Gailtalkristallin und an seiner Begrenzung. Ph. D. thesis, Universität Graz, Graz, 204 pp.

von Blanckenburg, F., 1992. Combined high-precision chronometry and geochemical tracing using accessory minerals: applied to the Central-Alpine Bergell intrusion (central Europe). Chem. Geol., 100: 19–40.

von Blanckenburg, F. and Davies, J.H., 1995. Slab breakoff: a model for syncollisional magmatism and tectonics in the Alps. Tectonics, 14: 120–131.

von Blanckenburg, F. and Davies, J.H., 1996. Feasibility of double slab breakoff (Cretaceous and Tertiary) during the Alpine convergence. Eclogae Geol. Helv., 89: 111–127.

Wagreich, M., 1995. Subduction tectonic erosion and Late Cretaceous subsidence along the northern Austroalpine margin (eastern Alps, Austria). Tectonophysics, 242: 63–78.

Wagreich, M. and Faupl, P., 1994. Palaeogeography and geodynamic evolution of the Gosau Group of the Northern Calcareous Alps (Late Cretaceous, Eastern Alps, Austria). Palaeogeogr., Palaeoclimatol., Palaeoecol., 110: 235–254.

Werling, E., 1992. Tonale-, Pejo- und Judikarien-Linie: Kinematik, Mikrostrukturen und Metamorphose von Tektoniten aus räumlich interferierenden aber verschiedenaltrigen Verwerfungszonen. Ph. D. thesis, ETH Zürich, Zurich, 276 pp.

Wernicke, B., 1995. Low-angle normal faults and seismicity: a review. J. Geophys. Res., 100(B10): 20,159–20,174.

Wortel, M.J.R. and Spakman, W., 1992. Structure and dynamics of subducted lithosphere in the Mediterranean region. Proc. K. Ned. Akad. Wetensch., 95: 325–347.

Ziegler, W., 1956. Geologische Studien in den Flyschgebieten des Oberhalbsteins (Graubünden). Eclogae Geol. Helv., 49: 1–78.